The Company *of*
Biologists

CORRECTION

The NAV2 homolog Sickie regulates F-actin-mediated axonal growth in *Drosophila* mushroom body neurons via the non-canonical Rac-Cofilin pathway

Takashi Abe, Daisuke Yamazaki, Satoshi Murakami, Makoto Hiroi, Yohei Nitta, Yuko Maeyama and Tetsuya Tabata

There was an error published in the supplementary material accompanying *Development* **141**, 4716-4728.

In Fig. S3B, it should read @29°C. The correct version of the figure now appears online.

The authors apologise to readers for this mistake.

DEVELOPMENT

RESEARCH ARTICLE

The NAV2 homolog Sickie regulates F-actin-mediated axonal growth in *Drosophila* mushroom body neurons via the non-canonical Rac-Cofilin pathway

Takashi Abe[1,2], Daisuke Yamazaki[1], Satoshi Murakami[1], Makoto Hiroi[1], Yohei Nitta[1], Yuko Maeyama[1] and Tetsuya Tabata[1,2,*]

ABSTRACT

The Rac-Cofilin pathway is essential for cytoskeletal remodeling to control axonal development. Rac signals through the canonical Rac-Pak-LIMK pathway to suppress Cofilin-dependent axonal growth and through a Pak-independent non-canonical pathway to promote outgrowth. Whether this non-canonical pathway converges to promote Cofilin-dependent F-actin reorganization in axonal growth remains elusive. We demonstrate that Sickie, a homolog of the human microtubule-associated protein neuron navigator 2, cell-autonomously regulates axonal growth of *Drosophila* mushroom body (MB) neurons via the non-canonical pathway. Sickie was prominently expressed in the newborn F-actin-rich axons of MB neurons. A *sickie* mutant exhibited axonal growth defects, and its phenotypes were rescued by exogenous expression of Sickie. We observed phenotypic similarities and genetic interactions among *sickie* and Rac-Cofilin signaling components. Using the MARCM technique, distinct F-actin and phospho-Cofilin patterns were detected in developing axons mutant for *sickie* and Rac-Cofilin signaling regulators. The upregulation of Cofilin function alleviated the axonal defect of the *sickie* mutant. Epistasis analyses revealed that Sickie suppresses the LIMK overexpression phenotype and is required for Pak-independent Rac1 and Slingshot phosphatase to counteract LIMK. We propose that Sickie regulates F-actin-mediated axonal growth via the non-canonical Rac-Cofilin pathway in a Slingshot-dependent manner.

KEY WORDS: ***Drosophila* mushroom body, Axon development, F-actin, Microtubule, Neuron navigator/UNC-53, Rac-Cofilin pathway, Slingshot LIMK**

INTRODUCTION

During brain development, neurons undergo multiple morphological changes to form an elaborate neural network. The *Drosophila* mushroom body (MB), which forms bilaterally symmetric and dorsomedially bifurcated axonal lobe structures in the central brain, has been well studied as a model of neuronal development (Awasaki et al., 2011; Ito et al., 1997; Lee et al., 1999; Miura et al., 2013; Zhu et al., 2006). Among various regulators of neuronal morphogenesis, ADF/Cofilin and Rac GTPase (Rac) are key molecules in controlling cytoskeletal remodeling in axonal development (Bernstein and Bamburg, 2010; Hakeda-Suzuki

et al., 2002; Hall and Lalli, 2010; Ono, 2007). Cofilin [Twinstar (Tsr) in *Drosophila*] plays an essential role as a regulator of axonal growth by severing and depolymerizing F-actin. Because Cofilin is activated by dephosphorylation by the Slingshot (Ssh) phosphatase and is inactivated by phosphorylation by LIMK, the loss of Ssh or excessive activation of LIMK results in an axonal growth defect (Mizuno, 2013; Ng and Luo, 2004). In *Drosophila*, Rac has been proposed to act as a bidirectional switch for signaling cascades. One signaling event is the canonical Rac-Pak-LIMK pathway to suppress Cofilin-dependent axonal growth. The overexpression of Pak, a downstream effector of Rac, induces axonal growth defects similar to those observed with LIMK overexpression. In addition, introducing one mutant copy of Rac or Pak suppresses the axonal defect induced by LIMK overexpression. Another signaling event is the Pak-independent non-canonical pathway to positively regulate axonal growth. Rac mutant animals show multiple MB axonal defects, but the axonal growth defect is alleviated by the exogenous expression of Rac1^{Y40C} (Ng et al., 2002), which lacks the ability to activate Pak but does not affect lamellipodia formation (Joneson et al., 1996; Lamarche et al., 1996). Furthermore, Rac1^{Y40C} overexpression remarkably suppressed the LIMK overexpression phenotype (Ng and Luo, 2004).

Although several pieces of evidence have suggested the importance of the non-canonical pathway and predicted the existence of its mediator, whether this pathway finally converges upon the downstream Cofilin pathway and subsequent F-actin reorganization remains unclear (Kligys et al., 2007; Nagata-Ohashi et al., 2004; Ng and Luo, 2004). Moreover, many biochemical studies have assessed the regulation of Cofilin function and F-actin states using *in vitro* systems; the endogenous changes in F-actin and Cofilin phosphorylation appear not to have been analyzed simultaneously with an internal control in developing brain. To address these issues, we searched for a novel factor that interacts with Rac-Cofilin signaling components and positively regulates MB axonal growth. We observed that Sickie, which has a calponin homology (CH) actin-binding domain and shares structural similarities with the human microtubule-associated protein (MAP) neuron navigator 2 (NAV2), showed prominent expression in F-actin-rich newborn MB axons and genetically interacted with Rac-Cofilin signaling regulators. Although Sickie was originally identified by genome-wide RNAi screening in *Drosophila* S2 cells and the report proposed the involvement of Sickie in the innate immune response (Foley and O'Farrell, 2004), in this report we focused on the function of Sickie in the regulation of Cofilin-mediated F-actin remodeling and propose an expanded model of regulatory mechanisms during axonal development (Ng and Luo, 2004).

[1]Institute of Molecular and Cellular Biosciences, University of Tokyo, Tokyo 113-0032, Japan. [2]Graduate Program in Biophysics and Biochemistry, Graduate School of Science, University of Tokyo, Tokyo 113-0033, Japan.

*Author for correspondence (ttabata@iam.u-tokyo.ac.jp)

RESULTS

Characterization of Sickie

To identify novel key factors that regulate MB axonal development through cytoskeletal remodeling we used *pBGay*, a *piggyBac* and *P*-element hybrid vector (gift of Claude Desplan, New York University, USA), to obtain a larger number of genomic insertion lines. Among the 2000 putative enhancer trap lines, we found that the *1631pBGay-gal4* line expressed the GFP reporter in developing MB α/β axons at ∼36 h after puparium formation (APF) (Fig. 1A). In this line, the *gal4* vector was inserted in the sixth intron of *sickie* (Fig. 1B). To examine the endogenous expression pattern of the Sickie protein, we generated a polyclonal antibody (Fig. 1C). We found that Sickie was broadly expressed in the neuropile of the developing brain (Fig. 1A″) and overlapped with the GFP signal in MB axons (Fig. 1A‴). As described in FlyBase, Sickie is a homolog of the human NAV2 MAP and shares several conserved domains and motifs: a CH actin-binding domain, coiled-coil (CC) motifs and an AAA ATPase (AAA) domain (Fig. 1C,D) (Akhmanova and Steinmetz, 2010; Banuelos et al., 1998; Erzberger and Berger, 2006; Galjart, 2010; Klein et al., 2011; Martinez-Lopez et al., 2005; Schmidt et al., 2009). SxIP EB1-binding motifs were identified with GENETYX.

To test the requirement of Sickie in axonal development, we generated several deletion mutant alleles by FLP-FRT-based mutagenesis (Fig. 1B) (Parks et al., 2004). *sickie^A* and *sickie^{A-2}* are *sickie* locus-specific deletion alleles. The sequence that encodes 510 amino acids corresponding to the third proline-rich region and the first CC motif was deleted in these *sickie* mutants. *sickie^{A-L2}* lacked the coding sequence corresponding to the CH domain, the first and second proline-rich regions, and the first SxIP motif. The *sickie^{A-L1}* and *sickie^{A-L3}* alleles lacked all domains deleted in the former three alleles. We also found a *piggyBac* transposon insertion allele, *sickie^{A384}*, by complementation tests with *sickie^A* and *Df(2L) ED1303*. *Df(2L)ED1303* is a large deficiency line that is lacking the entire coding sequence of *sickie* and the neighboring genes.

We found that the *sickie^{A/A384}* mutant displayed short axonal lobes compared with those of the control animal (Fig. 1E,F), although the morphology of the peduncle appeared normal. Because the axonal defect was most clearly distinguished in Fasciclin 2 (FasII)-labeled α/β axons (Crittenden et al., 1998), two categories were defined for the α/β lobe phenotype. If either the α or β axonal lobe failed to extend its axons beyond the half-line of a normally formed α or β lobe, the phenotype was classified as Class I. If both α and β lobes failed to extend their axons beyond the half-line of normal α/β lobes, the phenotype was classified as Class II (Fig. 1H). We compared the phenotypic severity among several *sickie* mutants and found that the penetrance of the *sickie^{A/A384}* mutant was nearly identical to that of the *sickie^{A-L1}/Df(2L)ED1303* mutant, an allelic combination of large deletions lacking the coding sequence including a start codon for Sickie (Fig. 1C,M). In addition, the *sickie^{A/A384}* mutants displayed defective ellipsoid body (EB) ring structures in each hemisphere of the central brain, presumably resulting from the axonal growth defect (Fig. 1I,J). We also detected a prominent Sickie signal in the core region of the peduncle, an area occupied by axons of newborn α/β neurons and marked by a reduced FasII signal (Fig. 1K-K″). By contrast, prominent Sickie expression was not detected in the *sickie^{A/A384}* mutants (Fig. 1L-L″). These results suggest that *sickie^A* and *sickie^{A384}* are loss-of-function alleles. In summary, we conclude that Sickie is strongly expressed in the axons of newborn α/β MB neurons, and mutants show axonal lobe extension defects suggesting that Sickie is required for the proper formation of MB axonal lobe structure.

Sickie is cell-autonomously required for the axonal growth of newborn MB neurons

To address whether Sickie regulates axonal development cell-autonomously, we performed single-cell MARCM analysis (Wu and Luo, 2006). Compared with the axons of wild-type α/β neurons (Fig. 2A), *sickie^A* mutant neurons failed to extend their branched axons to the lobe terminus (Fig. 2B). Next, we conducted rescue experiments to test the sufficiency of Sickie in MB axonal growth. First, we used *elav-gal4*, a pan-neuronal driver, to induce the expression of wild-type Sickie (*UAS-sickie^{WT}*). Sickie was broadly detected throughout neuronal structures, and the axonal growth defect was nearly fully suppressed, except for the β-lobe fusion phenotypes (Fig. 2C-C‴). This phenotype appears to be due to *sickie* overexpression because the phenotype was observed when *sickie* was expressed with *elav-gal4* in an otherwise wild-type background. Second, we introduced the *OK107-gal4* MB-expressing driver and observed the morphological rescue of MB axons (Fig. 2D-D‴). Third, to further dissect the spatiotemporal timing at which Sickie is required, we used *NP7175-gal4*, which drives gene expression in the α/β core neurons of adult MBs (Aso et al., 2009; Tanaka et al., 2008). We examined the *gal4* expression patterns of this driver line from the onset of puparium formation to the adult stage because α/β neurons are born at the beginning of the pupal stage (Lee et al., 1999). GFP expression was detected in the inner regions where young neurons reside in the FasII-labeled α/β lobes, although expression was weak, most likely owing to the delay of GFP expression (supplementary material Fig. S1). We found a significant rescue of the axonal defects with this driver (Fig. 2E, rightmost column), suggesting that Sickie expression in newborn α/β neurons is important for axonal growth. Similar rescue results were obtained using *UAS-mCherry::sickie^{WT}* (Fig. 2F). Finally, to examine whether the function of the AAA domain is required, we introduced a *sickie^{K1881A}* mutant form (*UAS-mCherry::sickie^{K1881A}*) and did not find significant rescue effects in either the *OK107-gal4*-based or *NP7175-gal4*-based experiments (Fig. 2G-H). Taken together, these results suggest that Sickie is cell-autonomously required in newborn MB neurons to positively regulate axonal growth through the function of the AAA domain.

Phenotypic similarities and genetic interaction among mutants for *sickie* and Rac-Cofilin signaling regulators

During development, newborn MB neurons extend their axons into the core region of the axonal bundle, an area in which the F-actin signal is prominent (Fig. 3A, asterisk) but the FasII signal is weak (Fig. 3A′) (Kurusu et al., 2002). We found that the prominent Sickie signal (Fig. 3A″) overlapped with F-actin at the core region in α/β axonal bundles (Fig. 3A‴), and Sickie has a CH actin-binding domain (Fig. 1C). These findings raise the possibility that Sickie plays a role in regulating the actin cytoskeleton in growing MB axons.

In a current model, Rac canonically signals to the downstream effector Pak, which activates LIMK to negatively regulate Cofilin-dependent axonal growth (Fig. 3B, red arrows) (Ng and Luo, 2004). Rac also signals to a Pak-independent pathway to promote axonal growth (Fig. 3B, green arrow), although the downstream signaling mechanism remains unclear (Fig. 3B, dotted lines). We found that the expression of constitutively active (CA) forms of Rac1 (*UAS-Rac1^{V12}*), Pak (*UAS-Pak^{Myr}*) and LIMK (*UAS-LIMK^{KD}*) all resulted in axonal growth defects (Ang et al., 2006; Hing et al., 1999; Luo et al., 1994). The CA mutants of Rac1 or Pak failed to extend axons to form peduncles and lobe structures, and we defined this axonal growth defect as 'posterior arrest', a more severe phenotypic class than Class I or Class II (Fig. 3D,E). This axonal defect was also
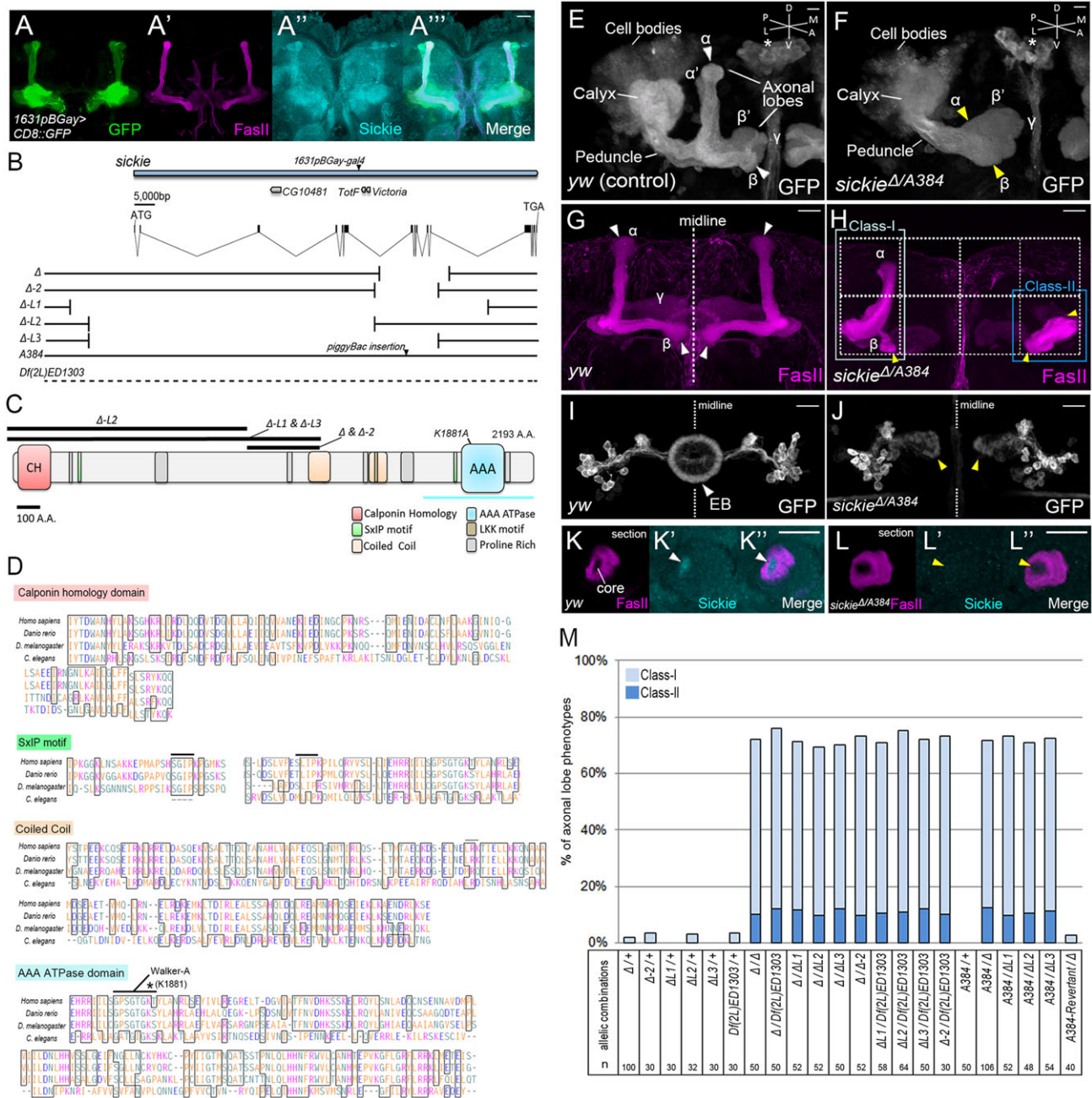
Fig. 1. Characterization of Sickie. (A-A‴) The expression patterns of CD8::GFP driven by *1631pBGay-gal4* and Sickie. GFP (A) and Sickie (A″) were detected in the developing brain, including MB axons labeled with FasII (A′). (B) Genomic structure of the *Drosophila sickie* locus. (C) Sickie domain structure. The regions deleted in each allele are indicated (see B). The light blue underline indicates the polypeptide sequence that was used as an antigen for generating the Sickie antibody. (D) Multiple alignment of homologous amino acid sequences in conserved domains. Sickie, human NAVs and *C. elegans* UNC-53 have evolutionarily conserved domains and motifs. (E,F) Adult MBs labeled with CD8::GFP driven by *OK107-gal4*. The white arrowheads indicate normal axonal lobes in the *yw* control. The yellow arrowheads indicate short axonal lobes in the *sickie$^{Δ/A384}$* mutant (see B for deletion). The white asterisks indicate the pars intercerebralis. Anterolateral view. (G,H) The α/β axonal lobes are labeled with FasII. The yellow arrowheads (H) indicate the termini of the defective lobes; compare with normal lobes in G (white arrowheads). Class II is a stronger phenotypic class than Class I. (I,J) The yellow arrowheads (J) indicate the split EB ring structure. EBs were labeled with CD8::GFP driven by *EB1-gal4*. (K-L″) Section images of developing axons at 72 h APF. The white arrowhead indicates prominent Sickie expression in the peduncle core region in which FasII expression is weak. The yellow arrowheads indicate loss of the Sickie signal in the peduncle core in the *sickie$^{Δ/A384}$* mutant. (M) Comparison of the phenotypic severities of various *sickie* mutants. Derived deletion mutants and *piggyBac* insertion mutant animals (see B) rarely showed defective α/β lobe phenotypes when the alleles were heterozygous in an *yw* control animal (*n*=30-100). By contrast, transheterozygous *sickie* mutant animals frequently showed axonal lobe growth defects (*n*=48-106). Scale bars: 20 µm.

observed in a *cofilin-RNAi* animal (Fig. 3G), suggesting that this phenotype reflects a significant impairment in Cofilin function. By contrast, the CA LIMK mutant frequently showed axonal growth defects at the lobe region but not the peduncle (Fig. 3F), and these

defects were similar to those observed in the *ssh$^{1-63}$* or *sickie$^{Δ/Δ}$* mutants (Fig. 3H,I). We also found that expression of dominant-negative Rac1 (*UAS-Rac1^{N17}*) frequently induced axonal growth defects in the lobe region (Fig. 3J) Although *sickie cofilin*
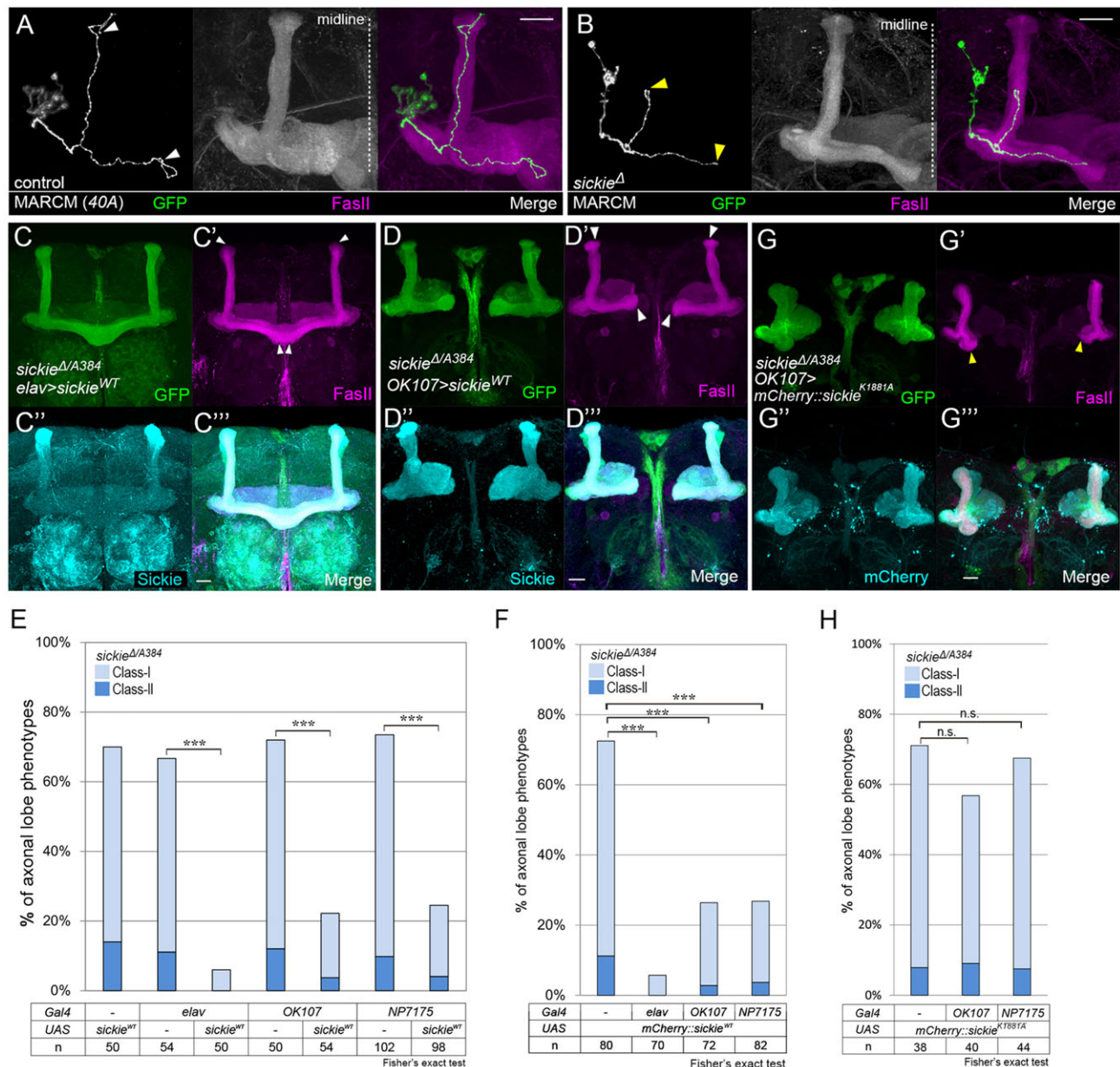
Fig. 2. Sickie is cell-autonomously required for the axonal growth of newborn MB neurons. (A,B) The yellow arrowheads (B) indicate that the *sickie*$^\Delta$ single-cell clone failed to extend branched axons to the α/β lobe terminus. *40A*: n=102, 2.94%. *sickie*$^\Delta$: n=104, 13.5%. (C-C‴) Phenotypic rescue of the *sickie* mutant phenotype by *elav-gal4*. (D-D‴) Sickie expression in MBs driven by *OK107-gal4* also rescued the mutant phenotype. (E) Quantification of the rescue effect. The specific expression of exogenous Sickie^{WT} in MBs by *elav-gal4*, *OK107-gal4* and *NP7175-gal4* significantly rescued the defects in *sickie*$^{\Delta/A384}$ mutants: ***P=4.40×10^{-11}, ***P=5.13×10^{-7} and ***P=2.30×10^{-12}, respectively. (F) Rescue effect of the *sickie*$^{\Delta/A384}$ mutant by mCherry::Sickie^{WT} expression. Similarly, the axonal defects were rescued by the following distinct *gal4* drivers: *elav-gal4*, ***P=2.84×10^{-18}; *OK107-gal4*, ***P=1.90×10^{-8}; and *NP7175-gal4*, ***P=8.66×10^{-9}. (G-G‴) Failure of phenotypic rescue by mCherry::Sickie^{K1881A} expression driven by *OK107-gal4*. The yellow arrowheads indicate short and malformed α/β axonal lobes (G′). (H) Rescue effect by mCherry::sickie^{K1881A} expression. Neither *OK107-gal4*- nor *NP7175-gal4*-dependent induction of Sickie^{K1881A} significantly rescued the *sickie* mutant phenotype (P=0.250 and P=0.808, respectively). Scale bars: 20 μm.

heterozygous mutants did not show obvious axonal growth defects (Fig. 3K,K′) and *Rac1 Rac2 Mtl* heterozygous mutants showed the Class I phenotype most frequently (Fig. 3L,L′), *Rac sickie cofilin* triple-heterozygous mutants showed a dramatic increase in the penetrance of the posterior arrest, and this mutant always showed the split EB (Fig. 3M-N).

Taken together, these results suggest that *sickie* genetically interacts with the Rac-Cofilin pathway and demonstrates a possible involvement of Sickie in Cofilin-dependent F-actin regulation in MB axonal growth.

Distinct patterns of F-actin enrichment in developing axons mutant for *sickie* and Rac-Cofilin signaling regulators

If Sickie functions in Cofilin-dependent F-actin reorganization, the F-actin expression pattern would be altered in developing axons in the *sickie* mutant, as the *ssh* mutant shows increased F-actin signal in epithelial tissues, such as eye and wing discs, and in follicle cells in the egg chamber (Corrigall et al., 2007; Nagel et al., 2010; Niwa et al., 2002). As expected, a prominent increase in F-actin signal was detected in the core region of the defective α/β axonal lobe in the *sickie*$^{\Delta/A384}$ mutant (Fig. 4B′, asterisk) compared with the *yw*
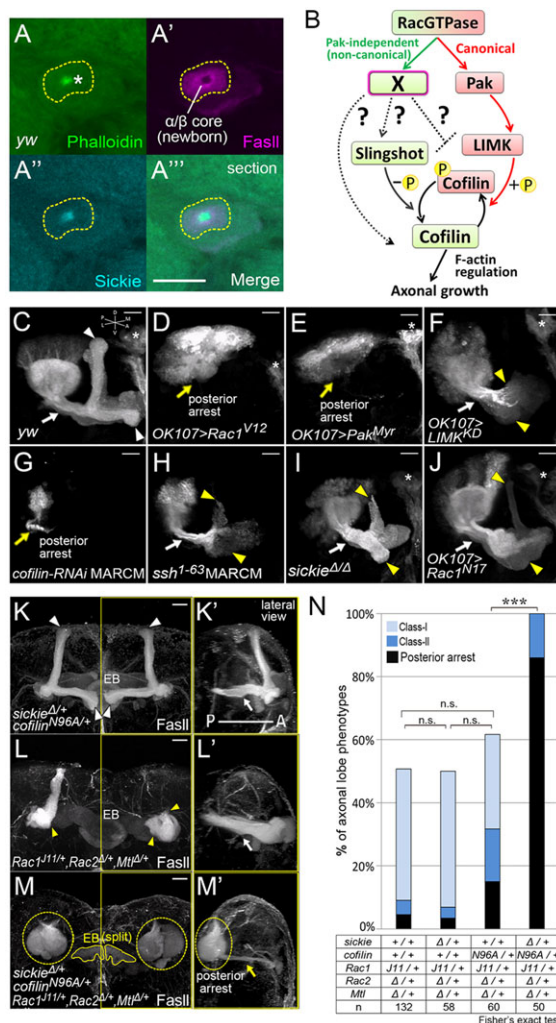
Fig. 3. Phenotypic similarities and genetic interaction among mutants for *sickie* and Rac-Cofilin signaling regulators. (A-A‴) Section images of developing MB axons at 72 h APF. (A‴) Overlapping F-actin (Phalloidin, asterisk) and Sickie signals were detected as complementary patterns with FasII in the core region. (B) The current Rac-Cofilin signaling model in MB axonal growth. The red arrows indicate the canonical Rac-Pak-LIMK pathway to suppress Cofilin-dependent axonal growth. The green arrow indicates the non-canonical Pak-independent pathway, mediated by unknown factor X, to positively regulate outgrowth. The dotted lines indicate possible signaling pathways. (C-J) 3D reconstructed images of typical mutant phenotypes for Rac-Cofilin signaling components. Each MB was labeled with CD8::GFP driven by *OK107-gal4*. The yellow arrows and arrowheads indicate axonal defects in the peduncle and lobe regions, respectively; whereas white arrows indicate the absence of a defect. The white asterisks indicate the pars intercerebralis. (K,K′) The *sickie cofilin* double-heterozygous mutants did not show obvious defects in α/β axonal lobes (K, white arrowheads), peduncle (K′, white arrow) and EB. (L,L′) *Rac1 Rac2 Mtl* heterozygous mutants displayed the Class I or II phenotype (L, yellow arrowheads). The peduncle (L′, white arrow) and EB formed normally. (M,M′) *Rac sickie cofilin* triple-heterozygous mutants frequently showed the posterior arrest phenotype (yellow circles). Thin peduncles (M′, yellow arrow) and split EBs (M, yellow outline) were observed. (N) A *Rac sickie cofilin* triple-heterozygous mutant showed a dramatic increase in the posterior arrest phenotype (rightmost column, ***P=8.64×10⁻⁸). Scale bars: 20 μm.

control animals (Fig. 4A′, asterisk). We also examined F-actin levels using the MARCM technique (Lee and Luo, 1999), which enabled us to detect even slight changes in F-actin levels by comparing a lobe containing homozygously mutated axons with a contralateral heterozygous lobe as an internal control within the

same brain (Fig. 4C′, white asterisk). A *sickie*[Δ] clone showed a slightly enhanced F-actin signal in the α/β lobe core region at ~72 h APF (Fig. 4C′, yellow asterisk). The mean intensity of the endogenous F-actin signal was significantly elevated in the α/β lobe containing the *sickie*[Δ] axons compared with that of the contralateral control lobe (Fig. 4F). These results suggest that Sickie is required for F-actin-mediated axonal growth of MB neurons.

Next, we examined mutant clones of *Ssh* and *LIMK*. An *ssh*[1-63] clone showed a stronger increase in F-actin signal at and around the core region of the α/β lobe (Fig. 4D′) than that of the *sickie*[Δ] clone, and the mean F-actin level was significantly elevated (Fig. 4G). By contrast, in a *LIMK*[KD] CA clone, although the prominent F-actin signal was similarly detected in the α/β lobe branching point, an additional signal increase was observed toward the distal region of the medial axons (Fig. 4E′). The mean F-actin signal level was also elevated in the *LIMK*[KD] mutant axons (Fig. 4H). Unlike the *sickie*[Δ], *ssh*[1-63] and *LIMK*[KD] mutants, the *Pak*[Myr] and *Rac1*[V12] clones displayed the posterior arrest phenotype (Fig. 4I″,J″) with ectopic regions of increased F-actin (Fig. 4I′,J′). A *cofilin-RNAi* clone also displayed the posterior arrest growth defect (Fig. 4K″) with a greater increase in F-actin (Fig. 4K′).

Distinct phospho-Cofilin expression patterns in developing axons mutant for *sickie* and Rac-Cofilin signaling regulators

To address whether Sickie is essential for the Cofilin-mediated F-actin reorganization, we next focused on the regulation of Cofilin, the critical converging point of the signaling cascades. MARCM analysis was also conducted to simultaneously detect changes in Cofilin phosphorylation and F-actin states in mutant axons to estimate Cofilin activity. Because Ssh directly activates Cofilin through dephosphorylation, we first examined whether increased phospho-Cofilin (P-Cofilin) signal was detectable in the axons of the *ssh*[1-63] clone. We used a P-Cofilin antibody (Zhang et al., 2011) and detected a broad increase in the P-Cofilin signal (Fig. 5A″, red outline) in the *ssh*[1-63] mutant axons compared with the internal control axons (Fig. 5A″, white outline), with a moderate increase in the F-actin signal (Fig. 5A′, yellow asterisk) at ~90 h APF. If Sickie is also essential for Cofilin dephosphorylation and Cofilin function is impaired in the *sickie*[Δ] mutant axons, a similar increase in the P-Cofilin signal would be observed. However, we did not detect obvious increases in P-Cofilin (Fig. 5B″) and F-actin (Fig. 5B′). Considering the moderate F-actin elevation in the *sickie*[Δ] clone (Fig. 4C′) compared with *ssh*[1-63] (Fig. 4D′), we reasoned that increased P-Cofilin would not be sufficiently high to detect immunohistochemically; therefore, we used immunoblotting. We found that relative P-Cofilin levels were increased ~1.8-fold (n=3) in the pupal brains of *sickie*[Δ/A384] mutants compared with control animals, as opposed to the cases of Ssh overexpression in which the corresponding signal was decreased as expected (Fig. 5C), suggesting that Sickie is involved in Cofilin dephosphorylation in developing axons.

Next, we tested the *LIMK*[KD] CA mutant clone. Previous *in vitro* studies showed that LIMK inactivates Cofilin through phosphorylation (Aizawa et al., 2001; Bernard, 2007; Endo et al., 2007; Nishita et al., 2005), and we found greater increases in the F-actin signal (Fig. 4E′,H). Therefore, we predicted a higher elevation of the P-Cofilin signal in the *LIMK*[KD] CA mutant. Surprisingly, however, we did not detect an obvious increase in P-Cofilin in the mutant axons (Fig. 5D″) despite continuous detection of the strong F-actin signal (Fig. 5D′), as compared with the *ssh*[1-63] mutant showing a moderate F-actin increase at the late pupal stage (Fig. 5A′). We further induced a *sickie*[Δ] *LIMK*[KD] CA
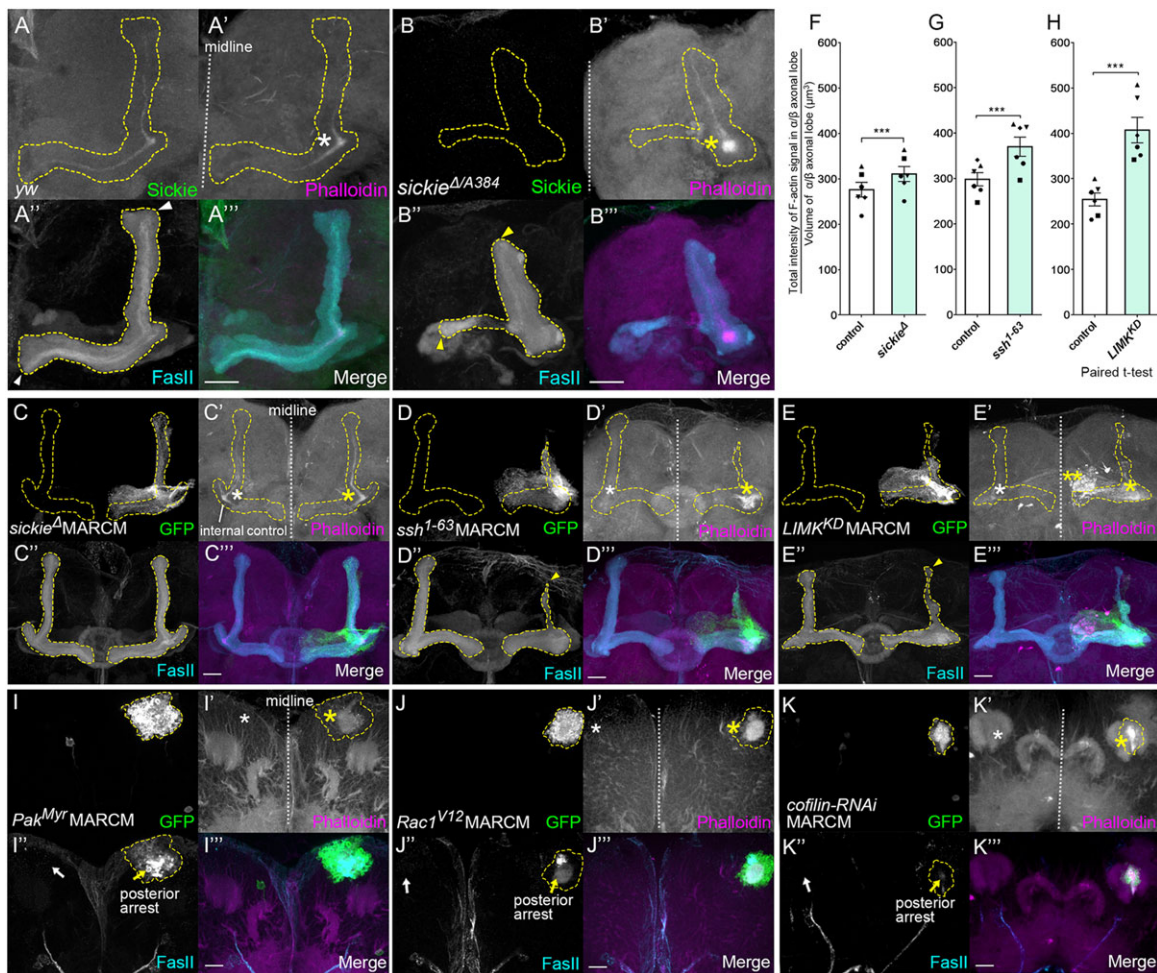
Fig. 4. Distinct patterns of increased F-actin in developing axons mutant for *sickie* and Rac-Cofilin signaling regulators. Yellow asterisks indicate increases in the F-actin signal at and around the lobe branching point of newborn α/β axons compared with the control region (white asterisks). Yellow arrowheads indicate axonal growth defects (compare with white arrowheads). (A-B‴) A prominent F-actin signal was detected in the core region of α/β axons in *sickie*$^{\Delta/A384}$ (B′) compared with the *yw* control (A′) at 72 h APF. (C-C‴) A *sickie*$^{\Delta}$ MARCM clone was labeled with GFP (C). A moderate F-actin increase was detected at and around the newborn α/β axons compared with the internal control region (C′). (D-D‴) In an *ssh*$^{1-63}$ clone, the F-actin signal was strongly detected at and around the α/β lobe branching point compared with the internal control (D′). (E-E‴) A *LIMK*^{KD} clone showed strong F-actin signals at and around the α/β lobe branching point (E′). The double asterisk indicates strong F-actin signal in the distal region of MB axons. (F-H) Quantification of increased F-actin signal in mutant axons. In all three genotypes, the mean F-actin signal intensities significantly increased in the α/β lobe containing mutant axons. Paired *t*-test, *n*=6 (represented by the different shapes; error bars indicate s.e.m.): *sickie*$^{\Delta}$, ***P=8.10×10^{-5}; *ssh*$^{1-63}$, ***P=3.26×10^{-4}; *LIMK*^{KD}, ***P=3.29×10^{-4}. (I-I‴) A *Pak*^{Myr} clone showing ectopic F-actin signal (I′) in the posteriorly arrested axons (I″). (J-J‴) A *Rac1*^{V12} clone similarly showed ectopic F-actin signal (J′) in the posteriorly arrested axons (J″). (K-K‴) A *cofilin-RNAi* clone showing strong F-actin signals (K′), with the posterior arrest axonal defect (K″). Scale bars: 20 μm.

double-mutant clone and detected elevated P-Cofilin levels in a part of the mutant axon bundle (Fig. 5E″, red outline). This P-Cofilin increase was modest yet higher than that of the *sickie*$^{\Delta}$ or *LIMK*^{KD} single mutant (Fig. 5B″,D″). These data suggest that F-actin levels do not always mirror Cofilin phosphorylation levels. Notably, activating upstream LIMK regulators by expressing *Pak*^{Myr} and *Rac1*^{V12} CA forms elevated both the P-Cofilin (Fig. 5F″,G″) and F-actin (Fig. 5F′,G′) signals.

In summary, these results suggest that Cofilin function is impaired in the *sickie* mutant and raise the possibility that Sickie is involved in the pathway counteracting canonical Rac-Pak-LIMK signaling.

Upregulation of Cofilin function in young MB neurons alleviates the axonal defect of the *sickie* mutant

To test the above hypothesis, epistatic studies were performed. We found significant rescue of the *sickie*$^{\Delta/A384}$ phenotype when wild-type (*UAS-cofilin*^{WT}) or active state-mimicking (*UAS-cofilin*^{S3A}) Cofilin was expressed in young α/β neurons (Fig. 6A,B,E), albeit less efficiently than Sickie itself (Fig. 2E). The overexpression of wild-type Ssh (*UAS-HA::ssh*^{WT}) but not the inactive form (*UAS-HA::ssh*^{CS}) also partially rescued the *sickie* phenotype (Fig. 6C,D,F). These results suggest that Sickie functions upstream of Ssh and Cofilin in MB axonal growth.

Sickie suppresses the axonal growth defect induced by LIMK overexpression

We next focused on the interaction between Sickie and LIMK. A previous study demonstrated the counteracting effect of Ssh and Pak-independent Rac1 against LIMK. The axonal growth defect induced by LIMK overexpression is significantly suppressed by the co-expression of Ssh^{WT} or Rac1^{Y40C} (Ng and Luo, 2004). In addition, the expression of LIMK^{WTM6} (*UAS-HA::LIMK*^{WTM6}), a stronger gain-of-function allele, frequently induces the Class II type
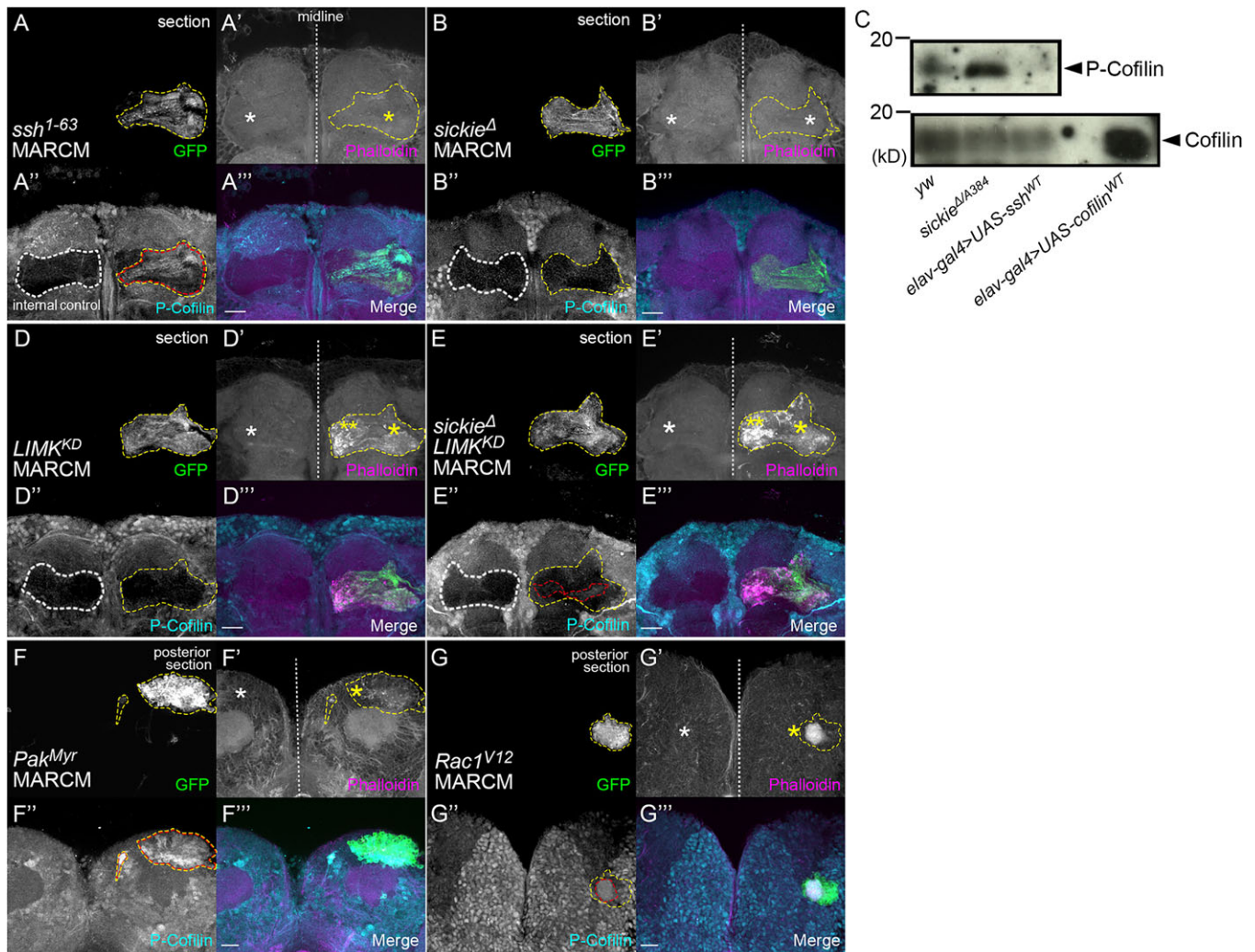
Fig. 5. Distinct P-Cofilin expression patterns in developing axons mutant for *sickie* and Rac-Cofilin signaling regulators. The yellow outlines indicate defective MB axons of mutant clones. The yellow asterisks indicate increased F-actin signal compared with the internal control region (white asterisks). The white outlines show basal level P-Cofilin signals in the internal control axons. The red outlines indicate increases in the P-Cofilin signal. Section images of anterior (A,B,D) or posterior (F,G) regions are shown. (A-A‴) An *ssh*[1-63] mutant clone showing broad elevation of the P-Cofilin signal in the defective axons (A″) with a moderately elevated F-actin signal (A′) at ~90 h APF. Note that the P-Cofilin detection pattern did not completely mirror that of GFP or F-actin. (B-B‴) A *sickie*[Δ] mutant clone did not show obvious increases in F-actin (B′) and P-Cofilin (B″) signals at the late pupal stage. (C) Lysates from pupal brains were analyzed by immunoblotting with antibodies specific for P-Cofilin and Cofilin. The relative mean P-Cofilin level was increased ~1.8-fold in the pupal brain of the *sickie*[Δ/Δ384] mutant compared with the *yw* control (n=3). The P-Cofilin signal was reduced in Ssh[WT]-expressing animals. The *elav-gal4* driver was used for transgene expression. Each mean P-Cofilin level was normalized to the mean total Cofilin intensity. (D-D‴) A *LIMK*[KD] constitutively active (CA) mutant clone also did not show a prominent P-Cofilin increase (D″), whereas F-actin elevation (D′) was continuously detected, unlike in the *ssh* mutant. (E-E‴) A *sickie*[Δ] *LIMK*[KD] CA clone showed a moderate P-Cofilin increase in part of the mutant axons (E″, red outline) with increased F-actin (E′, yellow asterisks). (F-F‴) A *Pak*[Myr] CA clone showed elevated P-Cofilin signal (F″) with ectopic F-actin signal (F′) in the posteriorly arrested axons. (G-G‴) A *Rac1*[V12] CA clone also showed elevated P-Cofilin (G″) and F-actin (G′) signals with the posterior arrest axonal defect. Scale bars: 20 µm. Images free of markings are shown in supplementary material Fig. S2.

axonal growth defect with a remarkable increase in F-actin level (Fig. 7A-A‴) (Ng, 2008). We found that Ssh[WT] or Rac1[Y40C] expression suppressed the strong defects in both the F-actin level and morphological phenotype induced by LIMK[WTM6] (Fig. 7B-C‴). If Sickie functions in the Pak-independent pathway to facilitate Cofilin function by similarly counteracting LIMK, the strong F-actin increase and axonal defects would be alleviated. We found this to be the case; Sickie[WT] expression reduced the elevated F-actin signal and rescued the defect in medial axon growth, although complete morphological rescues were rarely observed in the dorsal axons (Fig. 7D-D‴,F). Such suppressions were not observed when Sickie[K1881A] was expressed (Fig. 7E-F).

Sickie is required for Pak-independent Rac1 and Ssh to counteract LIMK

Based on the above results, we hypothesized that Sickie relays the non-canonical Rac pathway signal to Ssh to facilitate Cofilin function. To test this hypothesis, we examined whether Sickie is necessary for the counteracting effect of Pak-independent Rac1 or Ssh against LIMK (Fig. 7B,C). The counteracting effects by Rac1[Y40C] and Ssh[WT] would be diminished when Sickie function is lost. The results were consistent with this hypothesis; the counteracting effects of Rac1[Y40C] and Ssh[WT] were suppressed in the absence of Sickie, as the F-actin signals remained elevated (Fig. 7G′,I′, compared with 7C′,B′, respectively), and the axonal
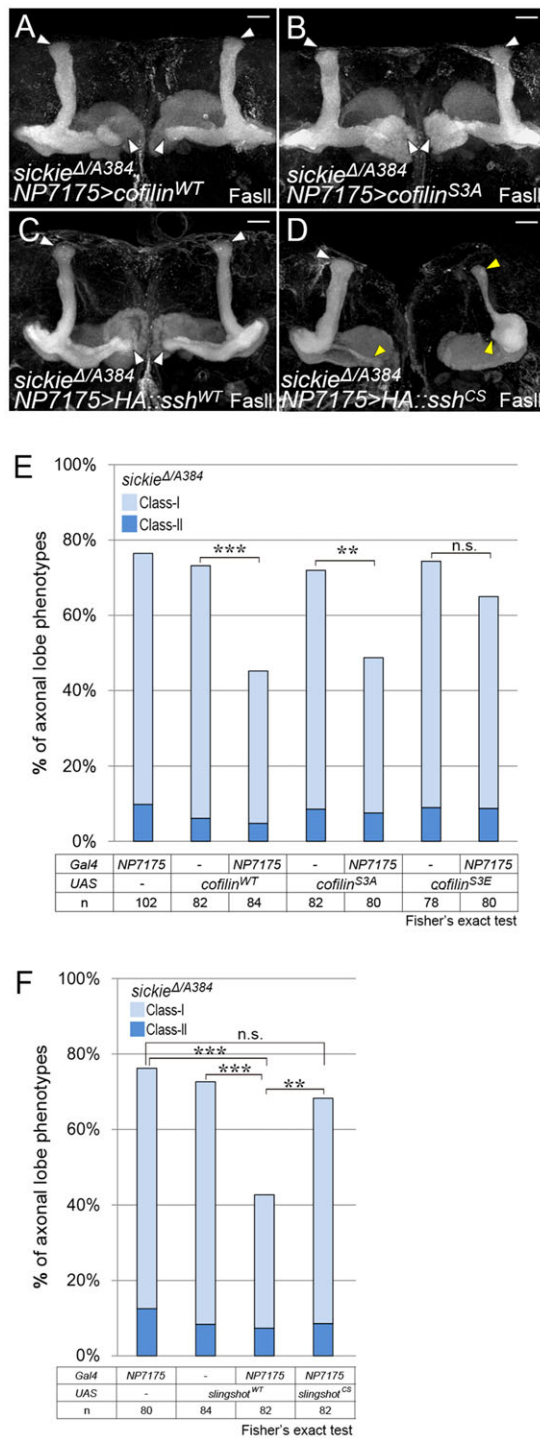
Fig. 6. Upregulation of Cofilin function in newborn MB neurons alleviates the axonal defect of the *sickie* mutant. (A,B) Forced expression of Cofilin[WT] (A) or Cofilin[S3A] (B) driven by *NP7175-gal4*, an α/β core driver, partially rescued the axonal growth defect in a *sickie[Δ/A384]* mutant. (C,D) The *sickie[Δ/A384]* mutant was also partially rescued by Ssh[WT] expression (C) but not by Ssh[CS] expression (D; yellow arrowheads). (E) Quantification of rescue effects of upregulation of Cofilin function. Expression of Cofilin[WT] or Cofilin[S3A] resulted in a significant reduction in the penetrance of the *sickie[Δ/A384]* axonal phenotype: Cofilin[WT], ***$P=2.87 \times 10^{-4}$; Cofilin[S3A], **$P=2.22 \times 10^{-3}$; Cofilin[S3E], $P=0.228$; Fisher's exact test. (F) Quantification of the rescue effect of Ssh overexpression on the *sickie[Δ/A384]* mutant phenotype. Ssh[WT] expression significantly rescued the defect: *NP7175/NP7175>ssh[WT]*, ***$P=1.50 \times 10^{-5}$; *NP7175/NP7175>ssh[CS]*, $P=0.295$; *ssh[WT]/NP7175>ssh[WT]*, ***$P=1.45 \times 10^{-4}$; *NP7175>ssh[WT]/NP7175>ssh[CS]*, **$P=1.59 \times 10^{-3}$; Fisher's exact test. Scale bars: 20 μm.

defects were not rescued (Fig. 7G,I, compared with 7C,B, and 7H,J, respectively). These results suggest that Sickie is required for both Pak-independent Rac1 and Ssh to counteract LIMK in MB axonal growth.

Sickie regulates Cofilin-mediated axonal growth in an Ssh-dependent manner

As shown previously in the simple Gal4-UAS system (Fig. 7A,A′,D,D′), increased F-actin and axonal defects caused by the overexpression of LIMK[WTM6] (Fig. 8A,A′) were also suppressed by the co-expression of Sickie[WT] in the MARCM system (Fig. 8B,B′). We examined whether this suppression by Sickie was dependent on Ssh by introducing an *ssh[1-63]* mutation into the MARCM system. *LIMK[WTM6] sickie[WT] ssh[1-63]* triple-mutant clones showed highly elevated F-actin (Fig. 8C′, asterisk) and P-Cofilin (Fig. 8D″, red outline) signals with the posterior arrest axonal defect (Fig. 8C″″), and the phenotypes were indistinguishable from those of a *LIMK[WTM6] ssh[1-63]* double-mutant clone (Fig. 8E′,E″,E″″), suggesting that Sickie functions upstream of Ssh in counteracting LIMK. This posterior arrest axonal defect of the *LIMK[WTM6] ssh[1-63]* mutant (Fig. 8E″″) was stronger than that of the *LIMK[WTM6]* (Fig. 8A) or *ssh[1-63]* (Fig. 3H) single-mutant clones and reminiscent of that of the *cofilin-RNAi* clone (Fig. 3G), indicating that Cofilin was nearly fully inactivated in the *LIMK[WTM6] ssh[1-63]* double mutant.

DISCUSSION
Role of the non-canonical Rac-Cofilin pathway in F-actin-mediated axonal growth

By combining the MARCM technique with epistatic analysis, we demonstrated that Sickie regulates the axonal growth of *Drosophila* MB neurons via the non-canonical Rac-Cofilin pathway. We propose the following model (Fig. 9). In wild type, Sickie relays the non-canonical pathway signal to Ssh (green arrows) to facilitate F-actin-mediated axonal growth by counteracting the canonical signal (red arrows). In a *sickie* mutant, mediation of the non-canonical pathway is defective, which causes an imbalance in the regulation of Cofilin activity. Because neurons are morphologically polarized and the amount of actin is limited in each cell, the growing axons may efficiently control actin recycling by facilitating F-actin turnover (Bugyi and Carlier, 2010) by balancing between the non-canonical and canonical pathways. Consistently, we have found a stronger axonal growth defect with increased P-Cofilin in the *LIMK[WTM6] ssh[1-63]* and *sickie[A] LIMK[KD]* double-mutant animals (Fig. 8E″ and Fig. 5E″) than in the single mutants *ssh[1-63]*, *sickie[A]* and *LIMK[KD]* (Fig. 5A″,B″,D″). Cofilin activity might be decreased in the developing axons of these double mutants by the preponderance of the canonical pathway. If so, these results highlight an essential role of the non-canonical pathway to balance Cofilin activity in axonal growth.

Simultaneous detection of P-Cofilin and F-actin changes in developing axons

Unlike the clear elevation of P-Cofilin levels in the *ssh[1-63]* mutant (Fig. 5A″), constitutive activation of LIMK did not result in a similar increase in P-Cofilin (Fig. 5D″) despite F-actin elevation (Fig. 5D′). This apparent paradox might be explained by considering the positive regulation of Ssh by F-actin. The phosphatase activity of SSH-1L is F-actin dependent, and the addition of F-actin dramatically increases its phosphatase activity (Nagata-Ohashi et al., 2004; Yamamoto et al., 2006). In the *LIMK[KD]* mutant axons, endogenous Ssh may be activated by a large amount of F-actin and subsequently dephosphorylates Cofilin. Consistently, highly elevated signals of both F-actin and P-Cofilin
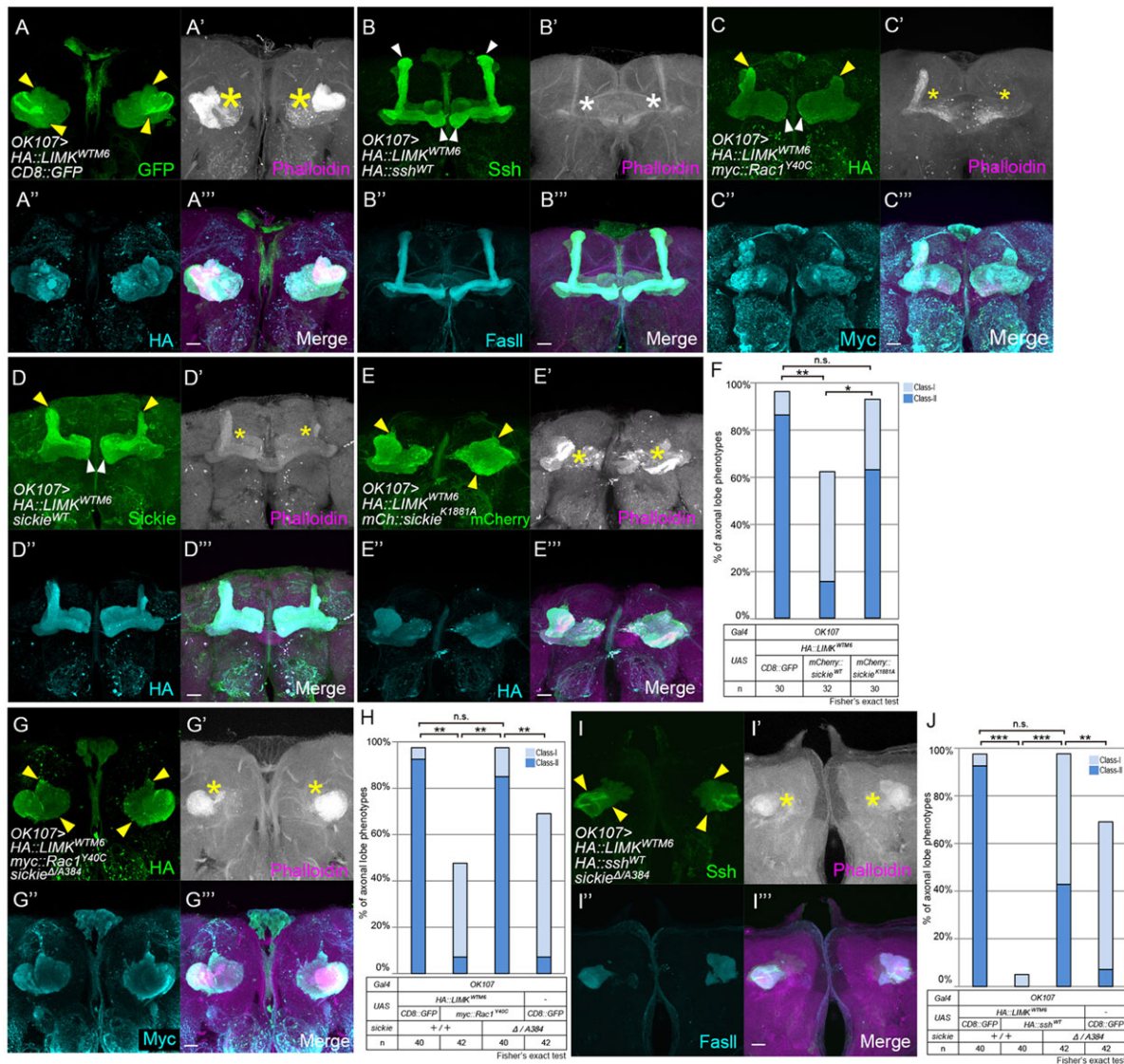
Fig. 7. Sickie suppresses the LIMK overexpression phenotype and is required for the functions of Pak-independent Rac1 and Ssh to counteract LIMK. The rescue effect on increased F-actin and the axonal growth defect were examined in the HA::LIMK^{WTM6} overexpression background. Yellow arrowheads indicate MB axon growth defects. Yellow asterisks indicate increased F-actin. (A-A‴) The Class II type axonal growth defect was induced by HA::LIMK^{WTM6} expression driven by *OK107-gal4* in both dorsal and medial axons (A). Highly elevated F-actin signals were detected in the defective MB axons (A′). (B-B‴) The axonal growth defects and F-actin elevation induced by HA::LIMK^{WTM6} were remarkably rescued by HA::Ssh^{WT} expression. Rescued α/β axons (B″) were observed. The elevated F-actin signal was reversed toward endogenous levels (B′). (C-C‴) The expression of Myc::Rac1^{Y40C}, which loses the ability to activate Pak by binding the CRIB motif, showed suppressive effects. The termini of rescued medial axons and defective dorsal axons are shown (C). A reduction in the elevated F-actin signal was observed (C′). (D-D‴) Sickie^{WT} expression also showed partial rescue effects. The white arrowheads indicate the termini of the rescued medial axons, and the yellow arrowheads indicate the termini of defective dorsal axons (D). A reduction in the elevated F-actin signal was observed (D′). (E-E‴) Expression of the mCherry::Sickie^{K1881A} AAA domain mutant form did not rescue either the dorsal and medial axonal defect (E) or the F-actin elevation (E′) induced by LIMK^{WTM6}. (F) Axonal defects were significantly suppressed by *mCherry::sickie^{WT}* expression but not by *mCherry::sickie^{K1881A}* driven by *OK107-gal4*. GFP/*sickie^{WT}*, **P=1.20×10^{-3}; GFP/*sickie^{K1881A}*, P=1.00; and *sickie^{WT}*/*sickie^{K1881A}*, *P=5.36×10^{-3}. (G-G‴) The rescue effect of Pak-independent Rac1 was abolished by Sickie loss of function. A strong F-actin signal was retained (G′) with the Class II type axonal growth defect (G). (H) Axonal defects were significantly suppressed by Pak-independent Rac1 expression but not in the *sickie$^{Δ/A384}$* background. GFP/*Rac1^{Y40C}*, **P=1.77×10^{-3}; GFP/*Rac1^{Y40C}sickie$^{Δ/A384}$*, P=1.00; *Rac1^{Y40C}*/*Rac1^{Y40C}sickie$^{Δ/A384}$*, **P=1.77×10^{-3}; and *Rac1^{Y40C}sickie$^{Δ/A384}$*/*sickie$^{Δ/A384}$*, **P=7.28×10^{-4}. (I-I‴) The rescue effect of Ssh was abolished by Sickie loss of function. F-actin signal elevation was still detected (I′) with the Class II type axonal defect (I). (J) Axonal defects were nearly completely rescued by *ssh^{WT}* expression but not in the *sickie$^{Δ/A384}$* background. GFP/*ssh^{WT}*, ***P=3.33×10^{-8}; GFP/*ssh^{WT}sickie$^{Δ/A384}$*, P=1.00; *ssh^{WT}*/*ssh^{WT}sickie$^{Δ/A384}$*, ***P=6.43×10^{-9}; and *ssh^{WT}sickie$^{Δ/A384}$*/*sickie$^{Δ/A384}$*. **P=7.08×10^{-4}. Scale bars: 20 μm.

were detected in the *LIMK^{WTM6} ssh$^{1-63}$* double-mutant clones (Fig. 8E′,E″). In this mutant, Cofilin activity was severely reduced by high phosphorylation levels due to constitutive LIMK activation and a lack of Ssh phosphatase activity, resulting in the posterior arrest severe axonal defect, similar to the *cofilin* knockdown mutant (Fig. 8E‴ and Fig. 3G). In addition, relatively moderate increases in

P-Cofilin signal were detected in the developing axons of the *sickie^{Δ} LIMK^{KD}* double mutant (Fig. 5E″). These results also support the model that Sickie functions in the same pathway as Ssh to positively regulate Cofilin function by counteracting the canonical Rac-Pak-LIMK pathway. Ssh might be downregulated in the *sickie* mutant axons due to defects in the mediation of Pak-independent Rac1
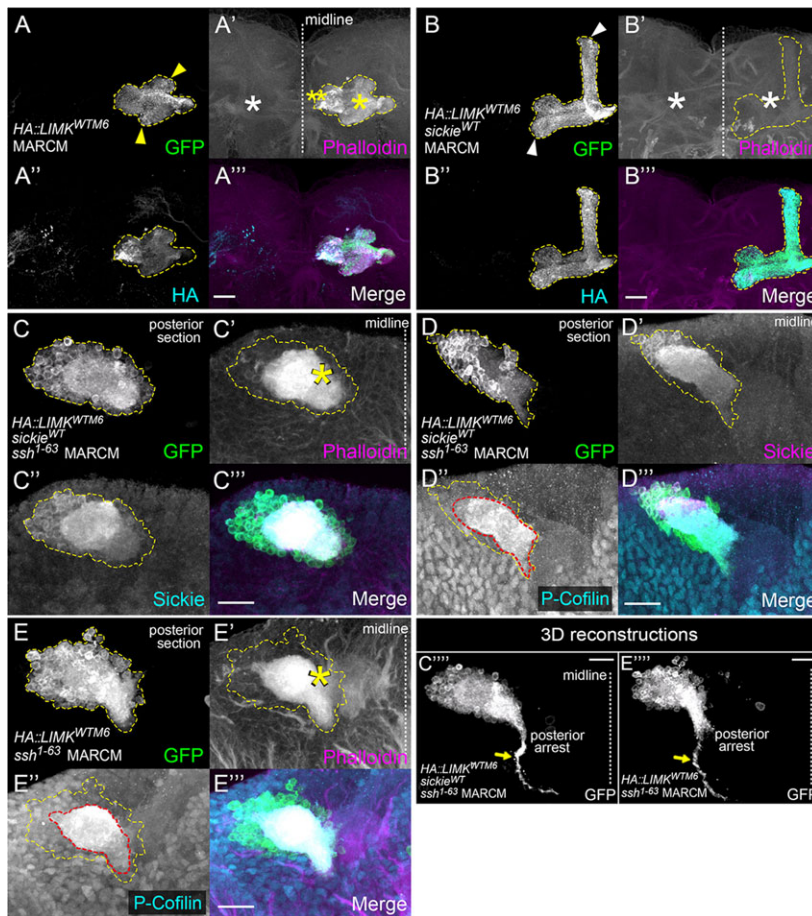
Fig. 8. Sickie regulates Cofilin-mediated axonal growth in an Ssh-dependent manner. F-actin or P-Cofilin patterns were examined in the anterior (A,B) or posterior (C-E) region of mutant brains at ~90 h APF. The yellow arrows and arrowheads indicate axonal defects in the peduncle and lobe regions, respectively. The yellow asterisks indicate increased F-actin. The red outlines indicate increased P-Cofilin. (A-A‴) An *HA::LIMK^WTM6* clone showed increased F-actin signal (A′) with both dorsal and medial axon growth defects (A). (B-B‴) An *HA::LIMK^WTM6 sickie^WT* double-mutant clone showed rescue effects in both F-actin signal (B′) and axonal growth (B). (C-D‴) In *HA::LIMK^WTM6 sickie^WT ssh^1-63* triple-mutant clones, highly elevated F-actin (C′) and P-Cofilin (D″) signals were detected in Sickie^WT-expressing axons (C″,D′). The posteriorly arrested axonal defect was observed (C‴). (E-E‴) A *LIMK^WTM6 ssh^1-63* double-mutant clone showed highly elevated F-actin (E′) and P-Cofilin (E″) signals in the posteriorly arrested axons (E‴). Scale bars: 20 µm.

function or in the interaction among Ssh and F-actin by the loss of Sickie. The similar increases in the P-Cofilin and F-actin signals and the similar posterior arrest phenotype in the *LIMK^WTM6 ssh^1-63* double-mutant clone and those of the *Pak^Myr* mutant clone are also consistent with results of *in vitro* studies that showed that SSH-1L is inactivated by Pak4 (Soosairajah et al., 2005; Van Troys et al.,

2008). Thus, in our model, Pak concurrently inactivates Ssh and activates LIMK in axonal growth (Fig. 9).

Possible function of Sickie

Whereas *ssh* or *cofilin* mutants are embryonic lethal and their mutant clones display developmental defects in non-neuronal tissues, *sickie*
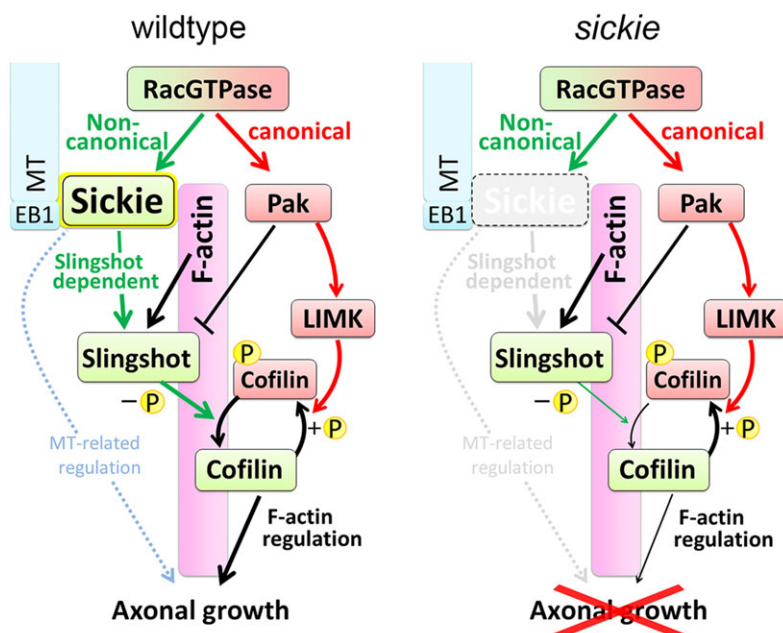

Fig. 9. Model for the involvement of Sickie in regulating axonal growth in MB neurons. In wild-type animals, the non-canonical Rac-Sickie-Ssh pathway (green arrows) counteracts the canonical Rac-Pak-LIMK pathway (red arrows) to facilitate F-actin-mediated axonal growth by balancing Cofilin activity. In *sickie* mutants, the relay of the non-canonical pathway is defective, which causes an imbalance in the regulation of Cofilin activity that impacts axonal growth.

mutants are not embryonic lethal, and conspicuous phenotypes are found only in the substructures of the central brain, such as MB and EB, implying that more elaborate mechanisms involving Sickie function are required for ensuring their proper development. Given that MB neurons exhibit a densely bundled axonal morphology, the growing MB axons might require Sickie to smoothly extend their neurites within the lobe core region by coordinating the dynamics of actin and microtubules (MTs). Sickie and human neuron navigator proteins (NAVs) have conserved EB1-binding motifs (Fig. 1D) (van Haren et al., 2009), and Sickie shows a genetic interaction with MT components (supplementary material Fig. S3). We found that double RNAi of *sickie* and *EB1* or *β-tubulin* both resulted in synergistic increases in the axonal defects. In addition, a recent cell biological study demonstrated a functional link between Cofilin and MTs (Flynn et al., 2012). Through its interaction with EB1 (Fig. 9, blue dotted arrow), Sickie might act as a navigator for the plus-end of MTs to link to the F-actin complex and thereby ensure elaborate neuronal wiring. To further elucidate the signaling mechanism, the relationships with other components of the Ssh-dependent Cofilin pathway need to be studied. Recent studies have revealed that PKD, 14-3-3 protein and Pak4 play key roles in suppressing Ssh function (Eiseler et al., 2009; Kligys et al., 2009; Spratley et al., 2011).

Finally, our preliminary data suggest a post-developmental role for Sickie. We have found that adult stage-specific knockdown of Sickie in MBs impairs olfactory memory (data not shown). Moreover, recent mammalian studies have suggested the possible involvement of NAVs and Cofilin in neurodegenerative disease (Maloney and Bamburg, 2007; Minamide et al., 2000). In Alzheimer's disease brains, the *NAV3* transcript level is elevated, and Cofilin-actin rod-shaped inclusions, which are formed by the hyperactivation of Cofilin, are enriched (Bernstein et al., 2012; Davis et al., 2011; Jang et al., 2005). Further studies are required to understand the wide variety of contributions of *sickie* and the general importance of this evolutionarily conserved gene in brain development and function.

MATERIALS AND METHODS

Drosophila strains

OK107-Gal4, *elav-Gal4*, *NP7175-Gal4* (Kyoto DGRC), *EB1-Gal4*, *UAS-mCD8::GFP*, $Rac1^{J11}Rac2^{\Delta}Mtl^{\Delta}$, UAS-$Rac1^{V12}$, *UAS-cMyc::Rac1*^{Y40C}, UAS-$Rac1^{N17}$, $cofilin^{N96A}$, UAS-$cofilin^{WT}$, UAS-$cofilin^{S3A}$, UAS-$cofilin^{S3E}$, UAS-Pak^{Myr}, $slingshot^{1-63}$, UAS-$HA::slingshot^{WT}$, UAS-$HA::slingshot^{CS}$, UAS-$HA::LIMK^{WTM6}$ (BDSC), UAS-$LIMK^{KD}$ (a gift from H. Hing, State University of New York at Brockport, USA), *yw; UAS-mCD8::GFP; OK107-Gal4* and *yw hs-flp UAS-mCD8::GFP; FRT82B tubP-Gal80/TM3; OK107-Gal4* (gifts from L. Luo, Stanford University, CA, USA), *yw; FRT40A* and *yw hs-flp UAS-mCD8::GFP; FRT40A tubP-Gal80; OK107-Gal4* (gifts from T. Lee, Janelia Research Campus, VA, USA), *UAS-sickie-RNAi* (VDRC, 31318), *UAS-cofilin-RNAi* (VDRC, 110599), *UAS-EB1-RNAi* (VDRC, 24451), *UAS-β-tubulin-RNAi* (VDRC, 24144) and *UAS-dicer2* (VDRC, 60009).

Histochemistry

Flies were dissected in a cold PBS solution and fixed in 4% formaldehyde for 40 min at room temperature. Immunostaining was performed as described previously (Huang and Kunes, 1996; Sato et al., 2006). The following antibodies were used: rabbit anti-GFP Alexa Fluor 488 conjugate (Molecular Probes; 1:2000); mouse anti-FasII (DSHB; 1:50); rabbit anti-DsRed (Takara #632496; 1:1000); mouse anti-HA (Covance; 1:500); rabbit anti-HA (Abcam #ab9110; 1:1000); rat anti-Slingshot (a gift from T. Uemura, Kyoto University, Japan; 1:1000); mouse anti-c-Myc (9B11, Cell Signaling #2276S; 1:10,000); rabbit anti-P-Cofilin (Signalway Antibody #11139-1; 1:200); anti-mouse Cy3, anti-rabbit Cy3, anti-rat Cy3, anti-mouse Cy5 and anti-mouse DyLight649 (all Jackson ImmunoResearch; 1:200); anti-rat Alexa Fluor 488, anti-rabbit Alexa

Fluor 660 and anti-rat Alexa Fluor 647 (all Molecular Probes; 1:200). Alexa Fluor 488 and 568 phalloidin were from Molecular Probes (#A12379, #A22283; 1:200). Images were captured and analyzed on a Zeiss LSM 710 confocal microscope and processed using Zeiss LSM Image Browser and Photoshop (Adobe Systems).

Identification and generation of *sickie* mutant alleles

The following insertion lines were used for the generation of the FLP-FRT deletion mutants. *sickie*^{A}: *sickie*^{d07725} and *sickie*^{d09251}. *sickie*$^{A-2}$: *sickie*^{f06833} and *sickie*^{e02238}. *sickie*$^{A-L1}$: *sickie*^{f07728} and *sickie*^{f04819}. *sickie*$^{A-L2}$: *sickie*^{f04737} and *sickie*^{f06833}. *sickie*$^{A-L3}$: *sickie*^{f04737} and *sickie*^{e02238}. The parental lines were obtained from the Exelixis Collection at Harvard Medical School. The *A384 piggyBac* element was inserted into the sixth intron of the *sickie* locus (Bellen, 2004; Ring and Garza, 2003) and the revertant allele, *sickie*^{A384Revertant}, was obtained through precise excision.

Generation of transgenic constructs

Total mRNA was extracted from dissected brains using the RNeasy Purification Kit (Qiagen), and reverse transcription was performed using the PrimeScript II High Fidelity RT-PCR Kit (Takara Bio). *sickie* cDNA was amplified using PrimeSTAR DNA polymerase (Takara Bio). The alignment of homologous sequences was performed using GENETYX (GENETYX Corporation). The mCherry (Clontech) coding sequence was inserted upstream of the *sickie*^{WT} or *sickie*^{K1881A} coding sequences using *Eco*RI/*Spe*I sites. An alanine mutation was introduced at the K1881 residue in the consensus ATP/GTP-binding (GxxxxGKS/T) motif in the AAA domain. These constructs were inserted into the pUAST (Brand and Perrimon, 1993) vector using *Eco*RI/*Xho*I sites. These plasmids were injected into *yw* embryos (BestGene).

Generation of Sickie antibody

A rat polyclonal anti-Sickie antibody was generated by Takara Bio. The antibody was raised against the 464 amino acids corresponding to residues 1734 to 2197 of the full-length Sickie protein. Anti-Sickie antibody was used at 1:1000.

Statistical test for genetic interaction

For the statistical analyses, two-sided Fisher's exact tests were used (Cyrus and Nitin, 1983). We made a 2×2 cross table that was composed of genotype A/B and the sum of the number of phenotypic samples (Class I+Class II+ posterior arrest)/number of non-phenotypic samples, and compared the difference in the percentages between the two groups. For multiple comparisons, Bonferroni correction was applied by the dividing significance levels by the number of genotypes in comparison.

Quantification of F-actin levels

F-actin signals in the α/β lobe region were combined to obtain the total F-actin intensity. The region of interest was extracted by the Surface program in Imaris software (Bitplane). In the mutant axons, the region of interest was further restricted by the GFP signal. The differences in the means of the average F-actin signal intensities were compared by a paired *t*-test.

Biochemistry

For the preparation of loading sample, pupal brains were dissected in TBS-T solution [Tris-buffered saline with Tween 20 tablets (pH 7.6), #T9142, TaKaRa] and collected in lysis buffer at −80°C. The following reagents were used for western blotting: rabbit anti-P-Cofilin (as above; 1:100), rabbit anti-Cofilin (rabbit polyclonal antisera to Tsr; a gift from T. Uemura; 1:2000) and mouse anti α-tubulin (#T9026 Sigma; 1:500,000) antibodies; Hybond-P PVDF membrane (GE Healthcare); PVDF Blocking Reagent (Toyobo, #NYPBR01). For signal detection, we used the ECL Prime Detection System (GE Healthcare) as per manufacturer's instructions. Data were quantified using ImageJ (NIH).

References

Aizawa, H., Wakatsuki, S., Ishii, A., Moriyama, K., Sasaki, Y., Ohashi, K., Sekine-Aizawa, Y., Sehara-Fujisawa, A., Mizuno, K., Goshima, Y. et al. (2001). Phosphorylation of cofilin by LIM-kinase is necessary for semaphorin 3A-induced growth cone collapse. *Nat. Neurosci.* **4**, 367-373.

Akhmanova, A. and Steinmetz, M. O. (2010). Microtubule +TIPs at a glance. *J. Cell Sci.* **123**, 3415-3419.

Ang, L.-H., Chen, W., Yao, Y., Ozawa, R., Tao, E., Yonekura, J., Uemura, T., Keshishian, H. and Hing, H. (2006). Lim kinase regulates the development of olfactory and neuromuscular synapses. *Dev. Biol.* **293**, 178-190.

Aso, Y., Grübel, K., Busch, S., Friedrich, A. B., Siwanowicz, I. and Tanimoto, H. (2009). The mushroom body of adult Drosophila characterized by GAL4 drivers. *J. Neurogenet.* **23**, 156-172.

Awasaki, T., Huang, Y., O'Connor, M. B. and Lee, T. (2011). Glia instruct developmental neuronal remodeling through TGF-beta signaling. *Nat. Neurosci.* **14**, 821-823.

Bañuelos, S., Saraste, M. and Djinović Carugo, K. (1998). Structural comparisons of calponin homology domains: implications for actin binding. *Structure* **6**, 1419-1431.

Bellen, H. J. (2004). The BDGP gene disruption project: single transposon insertions associated with 40% of Drosophila genes. *Genetics* **167**, 761-781.

Bernard, O. (2007). Lim kinases, regulators of actin dynamics. *Int. J. Biochem. Cell Biol.* **39**, 1071-1076.

Bernstein, B. W. and Bamburg, J. R. (2010). ADF/cofilin: a functional node in cell biology. *Trends Cell Biol.* **20**, 187-195.

Bernstein, B. W., Shaw, A. E., Minamide, L. S., Pak, C. W. and Bamburg, J. R. (2012). Incorporation of cofilin into rods depends on disulfide intermolecular bonds: implications for actin regulation and neurodegenerative disease. *J. Neurosci.* **32**, 6670-6681.

Brand, A. H. and Perrimon, N. (1993). Targeted gene expression as a means of altering cell fates and generating dominant phenotypes. *Development* **118**, 401-415.

Bugyi, B. and Carlier, M.-F. (2010). Control of actin filament treadmilling in cell motility. *Annu. Rev. Biophys.* **39**, 449-470.

Corrigall, D., Walther, R. F., Rodriguez, L., Fichelson, P. and Pichaud, F. (2007). Hedgehog signaling is a principal inducer of Myosin-II-driven cell ingression in Drosophila epithelia. *Dev. Cell* **13**, 730-742.

Crittenden, J. R., Skoulakis, E. M., Han, K. A., Kalderon, D. and Davis, R. L. (1998). Tripartite mushroom body architecture revealed by antigenic markers. *Learn. Mem.* **5**, 38-51.

Cyrus, R. M. and Nitin, R. P. (1983). A network algorithm for performing Fisher's exact test in r×c contingency tables. *J. Am. Stat. Assoc.* **78**, 427-434.

Davis, R. C., Marsden, I. T., Maloney, M. T., Minamide, L. S., Podlisny, M., Selkoe, D. J. and Bamburg, J. R. (2011). Amyloid beta dimers/trimers potently induce cofilin-actin rods that are inhibited by maintaining cofilin-phosphorylation. *Mol. Neurodegener.* **6**, 10.

Eiseler, T., Döppler, H., Yan, I. K., Kitatani, K., Mizuno, K. and Storz, P. (2009). Protein kinase D1 regulates cofilin-mediated F-actin reorganization and cell motility through slingshot. *Nat. Cell Biol.* **11**, 545-556.

Endo, M., Ohashi, K. and Mizuno, K. (2007). LIM kinase and slingshot are critical for neurite extension. *J. Biol. Chem.* **282**, 13692-13702.

Erzberger, J. P. and Berger, J. M. (2006). Evolutionary relationships and structural mechanisms of AAA+ proteins. *Annu. Rev. Biophys. Biomol. Struct.* **35**, 93-114.

Flynn, K. C., Hellal, F., Neukirchen, D., Jacob, S., Tahirovic, S., Dupraz, S., Stern, S., Garvalov, B. K., Gurniak, C., Shaw, A. E. et al. (2012). ADF/cofilin-mediated actin retrograde flow directs neurite formation in the developing brain. *Neuron* **76**, 1091-1107.

Foley, E. and O'Farrell, P. H. (2004). Functional dissection of an innate immune response by a genome-wide RNAi screen. *PLoS Biol.* **2**, e203.

Galjart, N. (2010). Plus-end-tracking proteins and their interactions at microtubule ends. *Curr. Biol.* **20**, R528-R537.

Hakeda-Suzuki, S., Ng, J., Tzu, J., Dietzl, G., Sun, Y., Harms, M., Nardine, T., Luo, L. and Dickson, B. J. (2002). Rac function and regulation during Drosophila development. *Nature* **416**, 438-442.

Hall, A. and Lalli, G. (2010). Rho and Ras GTPases in axon growth, guidance, and branching. *Cold Spring Harb. Perspect. Biol.* **2**, a001818.

Hing, H., Xiao, J., Harden, N., Lim, L. and Zipursky, S. L. (1999). Pak functions downstream of Dock to regulate photoreceptor axon guidance in Drosophila. *Cell* **97**, 853-863.

Huang, Z. and Kunes, S. (1996). Hedgehog, transmitted along retinal axons, triggers neurogenesis in the developing visual centers of the Drosophila brain. *Cell* **86**, 411-422.

Ito, K., Awano, W., Suzuki, K., Hiromi, Y. and Yamamoto, D. (1997). The Drosophila mushroom body is a quadruple structure of clonal units each of which contains a virtually identical set of neurones and glial cells. *Development* **124**, 761-771.

Jang, D.-H., Han, J.-H., Lee, S.-H., Lee, Y.-S., Park, H., Lee, S.-H., Kim, H. and Kaang, B.-K. (2005). Cofilin expression induces cofilin-actin rod formation and disrupts synaptic structure and function in Aplysia synapses. *Proc. Natl. Acad. Sci. USA* **102**, 16072-16077.

Joneson, T., McDonough, M., Bar-Sagi, D. and Van Aelst, L. (1996). RAC regulation of actin polymerization and proliferation by a pathway distinct from Jun kinase. *Science* **274**, 1374-1376.

Klein, C., Mikutta, J., Krueger, J., Scholz, K., Brinkmann, J., Liu, D., Veerkamp, J., Siegel, D., Abdelilah-Seyfried, S. and le Noble, F. (2011). Neuron navigator 3a regulates liver organogenesis during zebrafish embryogenesis. *Development* **138**, 1935-1945.

Kligys, K., Claiborne, J. N., DeBiase, P. J., Hopkinson, S. B., Wu, Y., Mizuno, K. and Jones, J. C. R. (2007). The slingshot family of phosphatases mediates Rac1 regulation of cofilin phosphorylation, laminin-332 organization, and motility behavior of keratinocytes. *J. Biol. Chem.* **282**, 32520-32528.

Kligys, K., Yao, J., Yu, D. and Jones, J. C. R. (2009). 14-3-3zeta/tau heterodimers regulate Slingshot activity in migrating keratinocytes. *Biochem. Biophys. Res. Commun.* **383**, 450-454.

Kurusu, M., Awasaki, T., Masuda-Nakagawa, L. M., Kawauchi, H., Ito, K. and Furukubo-Tokunaga, K. (2002). Embryonic and larval development of the Drosophila mushroom bodies: concentric layer subdivisions and the role of fasciclin II. *Development* **129**, 409-419.

Lamarche, N., Tapon, N., Stowers, L., Burbelo, P. D., Aspenström, P., Bridges, T., Chant, J. and Hall, A. (1996). Rac and Cdc42 induce actin polymerization and G1 cell cycle progression independently of p65PAK and the JNK/SAPK MAP kinase cascade. *Cell* **87**, 519-529.

Lee, T. and Luo, L. (1999). Mosaic analysis with a repressible cell marker for studies of gene function in neuronal morphogenesis. *Neuron* **22**, 451-461.

Lee, T., Lee, A. and Luo, L. (1999). Development of the Drosophila mushroom bodies: sequential generation of three distinct types of neurons from a neuroblast. *Development* **126**, 4065-4076.

Luo, L., Liao, Y. J., Jan, L. Y. and Jan, Y. N. (1994). Distinct morphogenetic functions of similar small GTPases: Drosophila Drac1 is involved in axonal outgrowth and myoblast fusion. *Genes Dev.* **8**, 1787-1802.

Maloney, M. T. and Bamburg, J. R. (2007). Cofilin-mediated neurodegeneration in Alzheimer's disease and other amyloidopathies. *Mol. Neurobiol.* **35**, 21-43.

Martínez-López, M. J., Alcántara, S., Mascaró, C., Pérez-Branguli, F., Ruiz-Lozano, P., Maes, T., Soriano, E. and Buesa, C. (2005). Mouse neuron navigator 1, a novel microtubule-associated protein involved in neuronal migration. *Mol. Cell. Neurosci.* **28**, 599-612.

Minamide, L. S., Striegl, A. M., Boyle, J. A., Meberg, P. J. and Bamburg, J. R. (2000). Neurodegenerative stimuli induce persistent ADF/cofilin-actin rods that disrupt distal neurite function. *Nat. Cell Biol.* **2**, 628-636.

Miura, S. K., Martins, A., Zhang, K. X., Graveley, B. R. and Zipursky, S. L. (2013). Probabilistic splicing of Dscam1 establishes identity at the level of single neurons. *Cell* **155**, 1166-1177.

Mizuno, K. (2013). Signaling mechanisms and functional roles of cofilin phosphorylation and dephosphorylation. *Cell Signal.* **25**, 457-469.

Nagata-Ohashi, K., Ohta, Y., Goto, K., Chiba, S., Mori, R., Nishita, M., Ohashi, K., Kousaka, K., Iwamatsu, A., Niwa, R. et al. (2004). A pathway of neuregulin-induced activation of cofilin-phosphatase Slingshot and cofilin in lamellipodia. *J. Cell Biol.* **165**, 465-471.

Nagel, A. C., Schmid, J., Auer, J. S., Preiss, A. and Maier, D. (2010). Constitutively active protein kinase D acts as negative regulator of the Slingshot-phosphatase in Drosophila. *Hereditas* **147**, 237-242.

Ng, J. (2008). TGF-beta signals regulate axonal development through distinct Smad-independent mechanisms. *Development* **135**, 4025-4035.

DEVELOPMENT

Ng, J. and Luo, L. (2004). Rho GTPases regulate axon growth through convergent and divergent signaling pathways. *Neuron* **44**, 779-793.

Ng, J., Nardine, T., Harms, M., Tzu, J., Goldstein, A., Sun, Y., Dietzl, G., Dickson, B. J. and Luo, L. (2002). Rac GTPases control axon growth, guidance and branching. *Nature* **416**, 442-447.

Nishita, M., Tomizawa, C., Yamamoto, M., Horita, Y., Ohashi, K. and Mizuno, K. (2005). Spatial and temporal regulation of cofilin activity by LIM kinase and Slingshot is critical for directional cell migration. *J. Cell Biol.* **171**, 349-359.

Niwa, R., Nagata-Ohashi, K., Takeichi, M., Mizuno, K. and Uemura, T. (2002). Control of actin reorganization by Slingshot, a family of phosphatases that dephosphorylate ADF/cofilin. *Cell* **108**, 233-246.

Ono, S. (2007). Mechanism of depolymerization and severing of actin filaments and its significance in cytoskeletal dynamics. *Int. Rev. Cytol.* **258**, 1-82.

Parks, A. L., Cook, K. R., Belvin, M., Dompe, N. A., Fawcett, R., Huppert, K., Tan, L. R., Winter, C. G., Bogart, K. P., Deal, J. E. et al. (2004). Systematic generation of high-resolution deletion coverage of the Drosophila melanogaster genome. *Nat. Genet.* **36**, 288-292.

Ring, B. and Garza, D. (2003). PBac constructs from the project genome wide dispersal of half-P elements in Drosophila using PiggyBac. FlyBase: FBrf0159884.

Sato, M., Umetsu, D., Murakami, S., Yasugi, T. and Tabata, T. (2006). DWnt4 regulates the dorsoventral specificity of retinal projections in the Drosophila melanogaster visual system. *Nat. Neurosci.* **9**, 67-75.

Schmidt, K. L., Marcus-Gueret, N., Adeleye, A., Webber, J., Baillie, D. and Stringham, E. G. (2009). The cell migration molecule UNC-53/NAV2 is linked to the ARP2/3 complex by ABI-1. *Development* **136**, 563-574.

Soosairajah, J., Maiti, S., Wiggan, O., Sarmiere, P., Moussi, N., Sarcevic, B., Sampath, R., Bamburg, J. R. and Bernard, O. (2005). Interplay between components of a novel LIM kinase-slingshot phosphatase complex regulates cofilin. *EMBO J.* **24**, 473-486.

Spratley, S. J., Bastea, L. I., Doppler, H., Mizuno, K. and Storz, P. (2011). Protein kinase D regulates cofilin activity through p21-activated kinase 4. *J. Biol. Chem.* **286**, 34254-34261.

Tanaka, N. K., Tanimoto, H. and Ito, K. (2008). Neuronal assemblies of the Drosophila mushroom body. *J. Comp. Neurol.* **508**, 711-755.

van Haren, J., Draegestein, K., Keijzer, N., Abrahams, J. P., Grosveld, F., Peeters, P. J., Moechars, D. and Galjart, N. (2009). Mammalian Navigators are microtubule plus-end tracking proteins that can reorganize the cytoskeleton to induce neurite-like extensions. *Cell Motil. Cytoskeleton* **66**, 824-838.

Van Troys, M., Huyck, L., Leyman, S., Dhaese, S., Vandekerkhove, J. and Ampe, C. (2008). Ins and outs of ADF/cofilin activity and regulation. *Eur. J. Cell Biol.* **87**, 649-667.

Wu, J. S. and Luo, L. (2006). A protocol for mosaic analysis with a repressible cell marker (MARCM) in Drosophila. *Nat. Protoc.* **1**, 2583-2589.

Yamamoto, M., Nagata-Ohashi, K., Ohta, Y., Ohashi, K. and Mizuno, K. (2006). Identification of multiple actin-binding sites in cofilin-phosphatase Slingshot-1L. *FEBS Lett.* **580**, 1789-1794.

Zhang, L., Luo, J., Wan, P., Wu, J., Laski, F. and Chen, J. (2011). Regulation of cofilin phosphorylation and asymmetry in collective cell migration during morphogenesis. *Development* **138**, 455-464.

Zhu, S., Lin, S., Kao, C.-F., Awasaki, T., Chiang, A.-S. and Lee, T. (2006). Gradients of the Drosophila Chinmo BTB-zinc finger protein govern neuronal temporal identity. *Cell* **127**, 409-422.
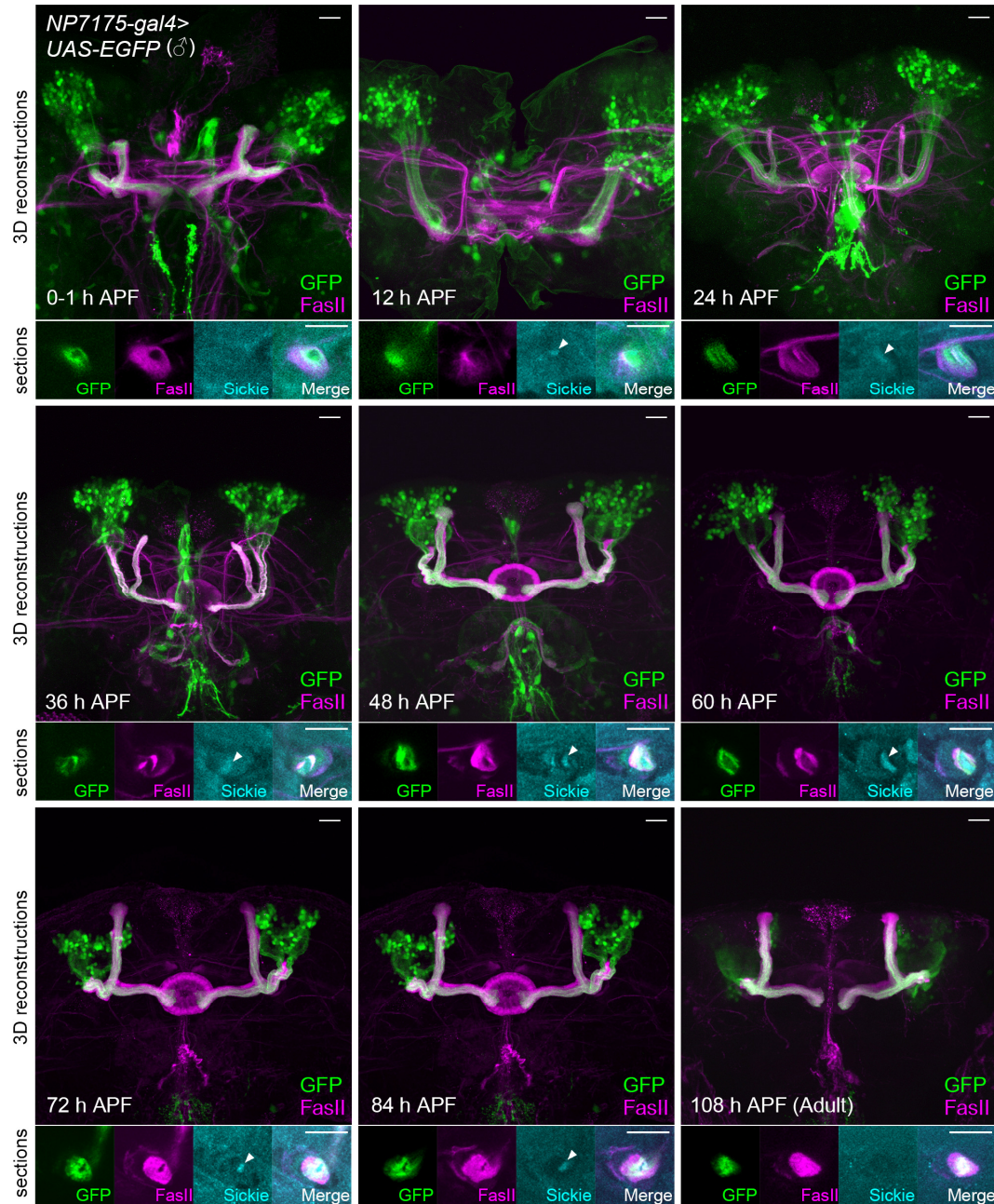
DEVELOPMENT

Fig. S1, related to Fig. 1

Fig. S1. The expression pattern of *NP7175-gal4* at pupal stage.

Throughout development, GFP signals were detected in the inner regions of FasII-labeled α/β axonal bundles. From 12 to 84 h APF, Sickie expression was prominently detected in the core regions of the axonal bundles (arrowheads) in which FasII signals were weak. We did not detect strong GFP signals in this exact core region of the peduncle. This result might be due to a delay in the Gal4/UAS system. Scale bar, 20 μm.
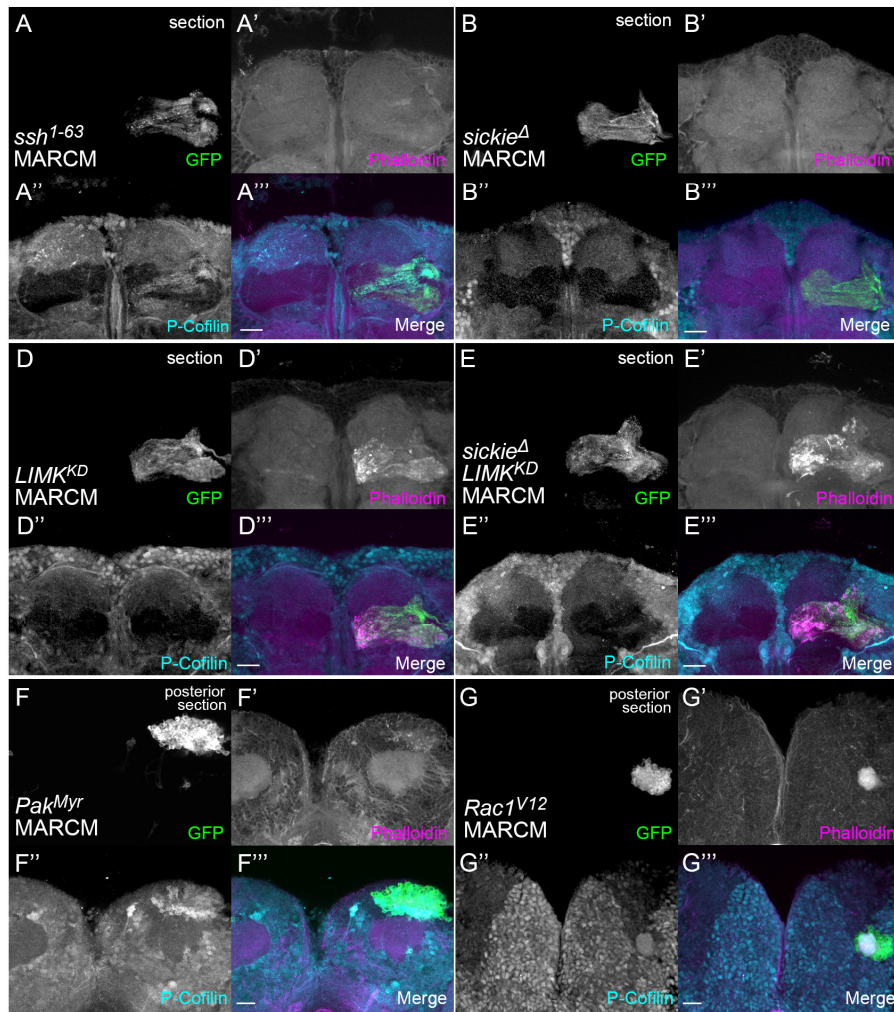
Fig. S2., related to Fig.5

Fig. S2. Duplicated Fig. 5 images free of markings.

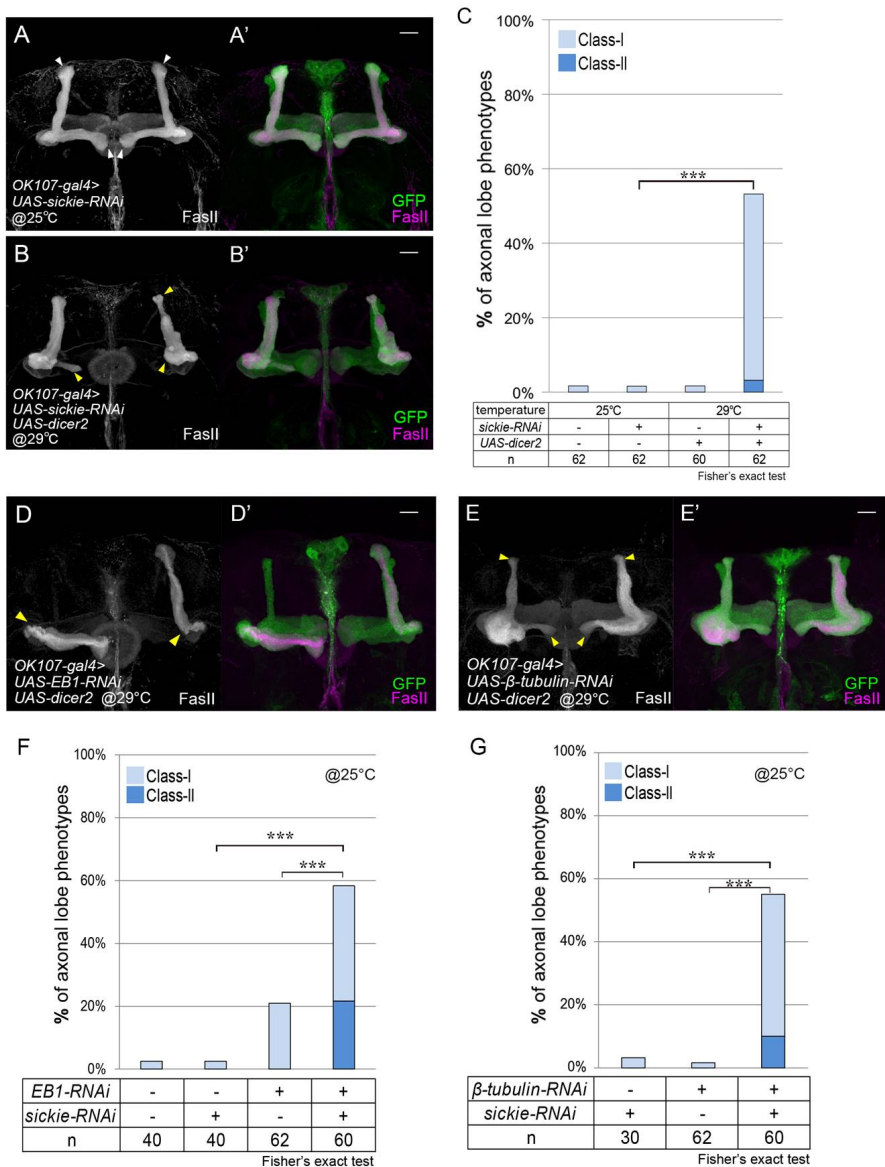Fig. S3, related to Discussion session

Fig. S3. Sickie genetically interacts with microtubule components.

(A-A') Any obvious axonal growth defect was not detected when *sickie-RNAi* knockdown was singly induced at 25°C. (B-B') Some RNAi-treated flies show axonal defects when RNAi was induced with *dicer-2* co-expression at 29°C. (C) The penetrance of the axonal defect was significantly increased when *dicer-2* was co-expressed and the flies were reared at 29°C. ***p=1.50×10^{-11}. (D-D',E-E') RNAi of either *EB1* or *β-tubulin* induced lobe

formation defects with *dicer-2* co-expression at 29°C. (F,G) Either *EB1-* or *β-tubulin-RNAi* also showed low penetrance of the axonal lobe formation defects at 25°C. However, compared with the single knockdown of *sickie*, the penetrance of the axonal defects synergistically increased in both RNAi treatments by combining with *sickie-RNAi,* even at 25°C. *sickie/sickie-EB1-RNAi*: ***p=1.54×10^{-9}, *EB1/sickie-EB1-RNAi*: ***p=3.63×10^{-5}, *sickie/sickie-β-tubulin-RNAi*: ***p=4.88×10^{-7}, and *β-tubulin/sickie-β-tubulin-RNAi*: ***p=3.25×10^{-12}. Scale bar, 20 μm.